CROSSING ESTIMATES ON GENERAL S-EMBEDDINGS

RÉMY MAHFOUF[A]

Abstract. We prove Russo-Seymour-Welsh type crossing estimates for the FK-Ising model on general s-embeddings whose origami map has an asymptotic Lipschitz constant strictly smaller than 1, together with a mild constraint on the level of local degeneracy of the embedding. This result extends the work of [5] and provides a general framework to prove that usual connection probabilities in boxes remain bounded away from 0 and 1. It is explained that one cannot prove similar estimates without an assumption of this kind on the origami map, and allows to propose some notion of critical model for generic planar graphs, that can be rephrased from the perspective of the associated propagator operator. Our theorem reproves along the way corresponding results in almost all already known setups but also treats new ones of interest.

1. Introduction, main results and perspectives

1.1. **General context.** The Ising model, introduced a century ago by Lenz, is one of the most studied models in statistical mechanics. Its planar version (i.e., the model on a planar graph with nearest-neighbor interactions) has received extensive attention from both physicists and mathematicians and gives rise to numerous local and global observables that can be computed exactly (see e.g. the monographs [24, 37, 39]). We focus in this article on the model with no exterior magnetic field, and contrary to usual conventions, we assign spins to *faces* (denoted by G°) of a planar graph G (whose vertices are denoted by $G^\bullet$). When G is a finite connected graph and $\beta > 0$ a positive number (called inverse temperature), one can attach to each edge $e \in E(G)$ separating the two faces $v^\circ_\pm(e) \in G^\circ$ a coupling constant $J_e > 0$ and construct a discrete probabilistic model, whose partition function is given by

$$\mathcal{Z}(G) \ := \sum_{\sigma : G^\circ \to \{\pm 1\}} \exp\big[\,\beta \sum_{e \in E(G)} J_e \sigma_{v^\circ_-(e)} \sigma_{v^\circ_+(e)}\,\big]. \tag{1.1}$$

The domain walls representation (see e.g. [7, Sec 1.2]) allows to rewrite $\mathcal{Z}(G)$ as

$$\mathcal{Z}(G) \ = \ 2 \prod_{e \in E(G)} (x(e))^{-1/2} \times \sum_{C \in \mathcal{E}(G)} \prod_{e \in C} x(e), \ \text{where } x(e) := \exp[-2\beta J_e]$$

and $\mathcal{E}(G)$ denotes the set of even subgraphs of G. By naturally identifying an edge e of G to the associated face $z(e)$ of the bipartite graph $\Lambda(G) := G^\bullet \cup G^\circ$, one can construct an *abstract parametrization* (i.e. a priori without any geometric interpretation) of the coupling constant $x(e)$ given by

$$\theta_{z(e)} \ := \ 2 \arctan x(e) \ \in \ (0, \tfrac{1}{2}\pi). \tag{1.2}$$

This abstract definition is purely combinatorial, and thus does *not* require to fix an embedding of G into $\mathbb{C}$: this fact was used by Chelkak to introduce the notion

[A] Université de Genève.
E-mail: `remy.mahfouf@unige.ch`.

of *s-embeddings* in [6, 5]. The overall goal of his construction is to provide an embedding procedure that allows to study large scale properties of weighted planar graphs (G, x) carrying critical or near-critical weights, depending on its collection of edge weights $(x(e))_{e\in E}$, including those locally very irregular, in a spirit similar to works such as e.g. circle packing embeddings [25], Tutte's embeddings [26] or more recently Cardy's embeddings [27]. The notion of (near-)criticality, which we understand here to be related to the existence of a non-trivial scaling limit, looks to be not yet proposed for generic planar graphs, except in particular cases, whose most famous examples are periodic lattices [15], the Z-invariant setup [4, 41] or Lis' circle packings [33]. Therefore, one aim of this paper is to propose one notion of criticality for general planar graphs, which can be read from the way the graph is embedded into the plane. As an example, the square lattice chosen with critical or off-critical weights will lead to embeddings with drastically different large scale properties (see [5, Figure 2]). More importantly, this allows to propose a notion of criticality (regarding crossing estimates) and reformulate it from the point of view of the spectral properties of the operator associated to the propagation equation (2.6) (see the question formulated in Section 1.4 for more details).

The route taken in [5] was to generalize the notion of discrete fermionic observables, in the spirit of the pioneering work of Smirnov [44, 43] that is based on discrete complex analysis techniques, by constructing an embedding procedure which is heavily tied to a combinatorial version of its obervables local relations. In particular, the construction extends to a much larger class of graphs than simply the isoradial or periodic ones, and we explore here its application regarding crossing probabilities. It is worth noting that the notion of s-embeddings is encapsulated in the more general framework of *t-embeddings* or *Coulomb gauges*, in the context of the bipartite dimer model [32, 13, 12]. This fact allows to benefit from the regularity theory of discrete harmonic and holomorphic functions developed in [13, Sec. 6], as well as an existence statement for finite planar graphs in [32, Sec. 7]. The s-embedding setup already proved its relevance in [5, Theorem 1.2] by settling the question of conformal invariance of the critical double-periodic graphs (the criticality condition in this setup was derived by Cimasoni and Duminil-Copin in [15, Theorem 1.1]) but also for regular graphs with an origami function satisfying $\mathcal{Q} = O(\delta)$ (see Definition 2.2 for more details). In the critical double-periodic case, even finding the correct canonical embedding [5, Lemma 2.3] and proving the convergence of FK interfaces to SLE(16/3) remained open for nearly a decade. This allowed one to go one step further regarding universality with respect to the local lattice details (see also similar results on critical and near critical isoradial grids for correlation functions in [14, 8, 41, 9, 40, 29, 11]). We hope that this framework will allow to study the Ising model in some random environments (see the example of a random triangulation decorated with the Ising model presented in Section 5.1), targeting (in the best case) critical random maps equipped with the Ising model -which is conjectured to converge to the Liouville Quantum Gravity (e.g. see [23])- as well as deterministic graphs with random coupling constants (e.g. $\mathbb{Z}^2$ with I.I.D. coupling constants studied numerically in [45]). We emphasize that the current paper does not treat the last two difficult questions.

1.2. **Definition of the embedding and the associated scale.** In order to keep the presentation compact, we postpone to Section 2 the precise definition of the construction of a proper s-embeddings $\mathcal{S}$ and give a rather informal and concrete review on what a tiling obtained following the construction of [5] looks like. One starts with a *weighted* planar graph (G, x) with the combinatorics of the plane (or of the sphere in the finite case), whose vertices are denoted by $G^\bullet$ and faces by G°. This graph is defined up to homeomorphism preserving the cyclic order of edges at each vertex. The graph $\Lambda(G) := G^\bullet \cup G^\circ$ can be viewed as a bipartite graph with edges connecting neighbors of different color in $\Lambda(G)$. A proper s-embedding of G can be viewed as a map $\mathcal{S} : \Lambda(G) \to \mathbb{C}$, such that all its edges are straight segments, and that all the faces of $\Lambda(G)$ (except maybe the outer face in the case of a finite graphs) are *tangential quadrilaterals*, i.e. each face delimited by the quadrilateral $(\mathcal{S}(v_0^\bullet)\mathcal{S}(v_0^\circ)\mathcal{S}(v_1^\bullet)\mathcal{S}(v_1^\circ))$ is tangential to a circle (more precisely the four lines containing the edges of that quad are tangential to a circle, which includes also the case of non-convex quads). The embedding is called *proper and non-degenerate* if different faces do not overlap each other and if none of the quadrilaterals $(\mathcal{S}(v_0^\bullet)\mathcal{S}(v_0^\circ)\mathcal{S}(v_1^\bullet)\mathcal{S}(v_1^\circ))$ is degenerated to a segment. It is possible to recover the Ising weight attached to an edge from the angles of the associated tangential quadrilateral using the relation (2.11). In particular, the overall idea is not based upon finding special weights that fit an embedded graph, but the other way around. Moreover, there are typically many different pictures for the same abstract graph, and all are as legitimate from the discrete complex analysis perspective. Those embeddings are stable under rotation, translation, homothecy and conjugations.

The second object of crucial importance in the s-embeddings framework is the so called origami map $\mathcal{Q}$, recalled in Definition 2.2. In words, the origami map $\mathcal{Q} : \Lambda(G) \to \mathbb{R}$ is a real valued function, defined up to additive constant, such that its increments between two neighboring vertices $\mathcal{S}(v^\bullet) \sim \mathcal{S}(v^\circ)$ are given by the local rule $\mathcal{Q}(\mathcal{S}(v^\bullet)) - \mathcal{Q}(\mathcal{S}(v^\circ)) := |\mathcal{S}(v^\bullet) - \mathcal{S}(v^\circ)|$. This means that $\mathcal{Q}$ adds edge lengths when going from vertices of $\mathcal{S}(G^\circ)$ to vertices of $\mathcal{S}(G^\bullet)$ and subtracts lengths when traveling in the other direction. This definition is indeed locally consistent as the alternate sum of edge-lengths in a tangential quadrilateral vanishes. It is easy to see that the function $\mathcal{Q}$ is automatically 1-Lipschitz (as a map in the $\mathcal{S}$ plane). In particular, it appears that some criticality of the model regarding crossing estimates can be analyzed using simply the behavior of the function $\mathcal{Q}$.

The preceding sentence looks at the first sight unclear, since to define the notion of large scale behavior, one should first define a notion of *scale* of the embedding. A priori, there is no natural notion of mesh size of a lattice in a highly irregular grid formed of tangential quadrilaterals. This can be done using the origami map $\mathcal{Q}$ and the assumption $\text{Lip}(\kappa,\delta)$, as originally defined in [13].

Assumption 1.1 ($\text{Lip}(\kappa,\delta)$)**.** *We say that the embedding $\mathcal{S}$ satisfies the assumption $\text{Lip}(\kappa,\delta)$ for some positive constant $\kappa < 1$ and some $\delta > 0$ if for any v, v' vertices of $\Lambda(G)$*

$$|\mathcal{Q}(v') - \mathcal{Q}(v)| \leq \kappa \cdot |\mathcal{S}(v') - \mathcal{S}(v)| \quad \textit{if} \quad |\mathcal{S}(v') - \mathcal{S}(v)| \geq \delta. \tag{1.3}$$

This allows to define the notion of *scale* of the embedding $\mathcal{S}$.

Definition 1.1. We say that an s-embedding $\mathcal{S}$ covering an open set $U \subseteq \mathbb{C}$ has a scale δ for the constant $\kappa < 1$ if

$$\delta = \delta^\kappa = \inf\{\tilde{\delta} > 0, \text{Lip}(\kappa, \tilde{\delta}) \text{ holds}\}. \tag{1.4}$$

In that case, we write $\mathcal{S} = \mathcal{S}^\delta = \mathcal{S}^{\delta^\kappa}$ (leaving the κ superscript unwritten).

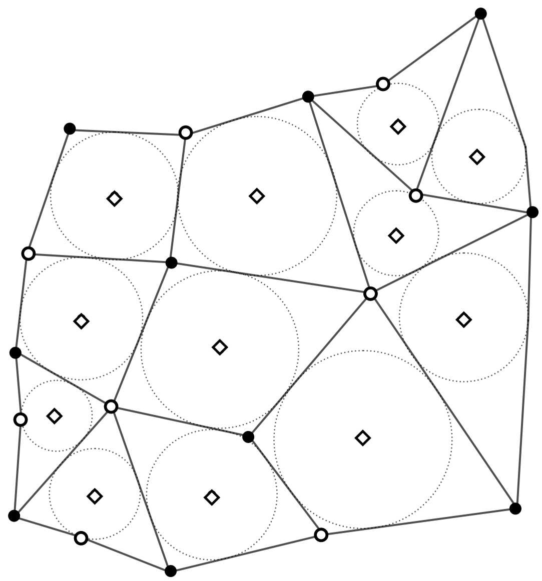

FIGURE 1. A piece of an s-embedding. The vertices of $G^\bullet$ are denoted by black dots, those of G° by white dots, and the center of tangential quadrilaterals with diamonds. The tangential circles are dashed.

In words, for some positive $\kappa < 1$, the scale of the embedding is the minimal length δ at which $\mathcal{Q}$ becomes κ Lipschitz. Regarding the results stated in this paper, the dependence in κ will play a role in the bounds of crossing estimates but not in the qualitative results themselves, as long as κ remains bounded away from 1. The dichotomy in behaviors of the statistical mechanics model happens when the origami map $\mathcal{Q}$ has an optimal Lipschitz constant (at large scale) strictly smaller than 1 or exactly equal to 1. In particular, when speaking about the scaling limit of a sequence of s-embeddings $(\mathcal{S}^\delta)_{\delta>0}$, it is taken along subsequences of s-embeddings $(\mathcal{S}^{\delta_n})_{\delta_n}$ with $\delta_n \to 0$ as $n \to \infty$ and all s-embeddings $\mathcal{S}^{\delta_n}$ satisfy $\text{Lip}(\kappa, \delta_n)$ for the *same* $\kappa < 1$. For grids with angles bounded from below and edge-lengths comparable to some δ (setup denoted by $\text{UNIF}(\delta)$ in [5]), the definition of the scale using $\text{LIP}(\kappa,\delta)$ coincides (up to an $O(1)$ factor) with δ. It is notable that there exist an even more natural way to embedd a planar graph as a space-like surface in the Minkowski space $\mathbb{R}^{2,1}$, taking the origami map as the third coordinate (see discussion in Section 5.2). The planar s-embedding setup is also stable under some naturally associated isometries in $\mathbb{R}^{2,1}$. This passage to $\mathbb{R}^{2,1}$ is not artificial as it is the natural environment to study the continuum scaling limit of fermionic observables in the s-embeddings context (see [5, Section 2.7]).

1.3. **Main Results.** In the current paper, we prove Russo-Seymour-Welsh crossing estimates (see [18, Sec. 5] for the statement on the critical square grid) for the

FK-Ising model on a sequence of proper s-embeddings that satisfy the condition $\text{Lip}(\kappa,\delta)$ for some $\kappa < 1$ (which we believe to be the crucial assumption of physical significance for theorems of the present paper to hold), together with a mild local constraint on the level of local degeneracy allowed in the considered embeddings (this is quantified by the assumption $\text{Exp-Fat}(\delta)$). The use of assumption of the kind $\text{Lip}(\kappa,\delta)$ is optimal and cannot be weakened, as we present graphs (which correspond to already known off-critical systems) where both $\text{Lip}(\kappa,\delta)$ (for any $\kappa < 1$) and the RSW property fail. Moreover, we explain in Section 5.2 that one *cannot* hope to prove crossing estimates bounded away from 0 and 1 without an assumption of the kind $\text{Lip}(\kappa,\delta)$. Indeed, one needs to prevent constructing a different embedding of the same statistical mechanics model, heavily stretched in one direction while its optimal Lipschitz constant gets arbitrarily close to 1.

In the present article *we do not rely upon any kind of bounded angle property, comparable edge-length assumptions, symmetry or translation invariance*, but use the scale defined via the assumption $\text{Lip}(\kappa,\delta)$ together with discrete complex analysis techniques. We answer a question of [5, Section 1.4 (I)] and treat the case $\mathcal{Q} \not\to 0$, removing drastically conditions on the local and global geometrical features of the embedding, providing one of the most flexible frameworks known to date where crossing estimates are available. In that setup, the system behaves qualitatively in a similar fashion as the usual critical model on the square lattice (existence of macroscopic wired clusters, polynomial decay of correlations, precompactness of FK interfaces, ect.)

As already mentioned, we believe that the only important assumption crucial to prove Theorems 1.1 and 1.2 is exactly $\text{Lip}(\kappa,\delta)$ (see the discussion made in Section 5.2). Still, our proof is based on discrete complex analysis techniques. Therefore, one needs to be able to prove precompactness of discrete s-holomorphic functions, which requires adding to $\text{Lip}(\kappa,\delta)$ a mild assumption denoted $\text{Exp-Fat}(\delta)$ that prescribes the local level of degeneracy that is allowed in the embeddings we work on. This restriction on the local structure of the embedding ensures precompactness of s-holomorphic functions via Theorem 2.19 and is stated now, following the formalism of [13, Assumption 1.2].

Assumption 1.2. *We say that a family of proper s-embeddings $(\mathcal{S}^\delta)_{\delta>0}$ satisfies the assumption* $\text{Exp-Fat}(\delta)$ *on an open subset $U \subset \mathbb{C}$ if for each $\gamma > 0$:*

after removing all quads $(\mathcal{S}^\delta)^\diamond(z)$ with $r_z \geq \exp(-\gamma\delta^{-1})$ from U, the maximal diameter of all vertex-connected components goes to 0 when $\delta \to 0$.

Translated in words, the assumption $\text{Exp-Fat}(\delta)$ means that there exists a positive function denoted $o_{\delta\to 0}(1)$, converging to 0 as $\delta \to 0$, such that the connected components of vertices attached to tangential quadrilaterals with a radius smaller than $\exp(-o_{\delta\to 0}(1)\delta^{-1})$ do not form macroscopic regions in the limiting regime. In all examples presented in this article, the assumption $\text{Exp-Fat}(\delta)$ is verified with a huge margin. From our perspective, the failure of the assumption $\text{Exp-Fat}(\delta)$ corresponds to drastic degeneracies of the obtained planar embedding that do not permit an analysis via the more flexible versions known to date of discrete complex analysis.

Under the assumptions $\text{Lip}(\kappa,\delta)$ and $\text{Exp-Fat}(\delta)$, we show that boxes of macroscopic size satisfy the usual Russo-Seymour-Welsh box crossing property for the associated FK-Ising model (see e.g. [18, Chapter 4] for precise definitions and relations between the spin-Ising model and the random cluster representation). The proof of such theorem starts with a proof of a lower bound for the magnetization of the spin-Ising model with 4 alternating boundary conditions.

Theorem 1.1. *Let $x_1 < x_2$, $y_1 < y_2$, $\mathcal{R} := (x_1, x_2) \times (y_1, y_2) \subset \mathbb{C}$, and $(\mathcal{S}^\delta)_{\delta>0}$ be s-embeddings satisfying the assumptions* $\text{Lip}(\kappa,\delta)$ *and* $\text{Exp-Fat}(\delta)$ *covering an open set containing $\overline{\mathcal{R}}$, for some fixed $\kappa < 1$.*
Let $\mathcal{R}^\delta = [\mathcal{R}(x_1, x_2; y_1, y_2)]^{\circ\bullet\circ\bullet}_{\mathcal{S}^\delta}$ be a discretization of $\mathcal{R}$ whose boundary approximates the boundaries of $\mathcal{R}$ as δ goes to 0. We consider the Ising model in $\mathcal{R}^\delta$ with wired boundary conditions on the approximations $(b^\delta c^\delta)^\circ$ and $(d^\delta a^\delta)^\circ$ of 'horizontal' segments and free boundary conditions the approximations $(a^\delta b^\delta)^\bullet$ and $(c^\delta d^\delta)^\bullet$ of the 'vertical' segments. Then one has

$$\liminf_{\delta\to 0} \mathbb{E}^{\circ\bullet\circ\bullet}_{\mathcal{R}^\delta}[\sigma_{(b^\delta c^\delta)^\circ}\sigma_{(d^\delta a^\delta)^\circ}] \ \geq \ \text{cst} \ > \ 0,$$

where the constant cst *only depends on κ and the ratio $|x_2 - x_1| \cdot |y_2 - y_1|^{-1}$.*

Proof. The theorem is a consequence of monotonicity with respect to boundary conditions (e.g. [18, Section 4] for reminders on those statements) and the proof in the case of the special discretizations constructed in Section 4. □

A similar theorem holds for the dual model, defined using Kramers-Wannier duality. The next theorem classically follows from Theorem 1.1. Given $u \in \mathbb{C}$ and $d > 0$, denote the annulus

$$\begin{aligned}\square(u, d) \ := \ &([\operatorname{Re} u - 3d, \operatorname{Re} u + 3d] \times [\operatorname{Im} u - 3d, \operatorname{Im} u + 3d]) \\ &\qquad \smallsetminus ((\operatorname{Re} u - d, \operatorname{Re} u + d) \times (\operatorname{Im} u - d, \operatorname{Im} u + d))\end{aligned}$$

and let $\mathbb{P}^{\text{free}}_{\square^\delta(u,d)}$ be the probability measure in the random cluster representation of the Ising model with free boundary conditions on both the outer and the inner boundaries of a discretization of $\square(u, d)$ by $\square^\delta(u, d)$. Then we have the following theorem:

Theorem 1.2. *There exists a constant $p_0 > 0$, only depending on κ, such that for all $u \in \mathbb{C}$, $d > 0$, and all s-embeddings $\mathcal{S}^\delta$ satisfying* $\text{Lip}(\kappa,\delta)$ *and* $\text{Exp-Fat}(\delta)$ *and covering the disc $B(u, 5d)$, one has*

$$\liminf_{\delta\to 0} \mathbb{P}^{\textit{free}}_{\square^\delta(u,d)}\big[\text{there exists a wired circuit in } \square^\delta(u, d)\big] \ \geq \ p_0.$$

A similar uniform estimate holds for the dual model.

Proof. Once Theorem 1.1 is derived, one can apply the strategy of [19, Proposition 2.10] recalled in detail in [5, Section 5.6].) □

In the case of s-embeddings satisfying $\text{Unif}(\delta)$, both theorems hold not only at macroscopic distances but also starting at distances comparable to δ. One can also note that the same proof works at mesoscopic scales compared to δ (e.g. δ^α for $0 < \alpha < 1$), modifying accurately the hypothesis $\text{Exp-Fat}(\delta)$ (see [5, Assumption 2.19]). It is even possible to weaken the local assumption $\text{Exp-Fat}(\delta)$ by a more global one using the presence of long circuits of 'fat' enough faces (with a large enough inner circle). Let us also emphasize that the results stated below are stated as lim inf, since coupling constant can be locally arbitrary large and thus among finite size boxes, the crossing probabilities can indeed be close to 0.

We explain now how to reformulate those theorems closer to their usual formulation regarding crossing probabilities in boxes of increasing size, aiming to simplify their understanding to percolation aficionados. Fix some $\kappa < 1$. Using a homothecy, one can rescale a finite proper s-embedding satisfying $\textsc{Lip}(\kappa,\delta)$ such that $\delta = 1$. Denote Λ_n the discretization of the square $[-n,n]^2$ by this s-embedding of mesh size 1. In that case, the hypothesis $\textsc{Exp-Fat}(\delta)$ can be reformulated in the following way:

There exist two functions $o_{n\to\infty}(1)$ and $\tilde{o}_{n\to\infty}(1)$ going to 0 as n goes to ∞ such that, after removing all quads $(\mathcal{S}^1)^\diamond(z)$ with $r_z \geq \exp(-o_{n\to\infty}(1)n)$ from Λ_{2n}, the maximal diameter of all vertex-connected components is $\tilde{o}_{n\to\infty}(1)$.

Then one can reformulate the previous theorems in the following way

(1) Consider the discretization of Λ_n with wired boundary conditions on the horizontal sides and free boundary conditions on the vertical sides. Then

$$\liminf_{n\to\infty} \mathbb{E}_{\Lambda_n}^{\circ\bullet\circ\bullet}[\sigma_{\mathrm{btm}^\circ}\sigma_{\mathrm{top}^\circ}] > \mathrm{cst}(\kappa) \tag{1.5}$$

(2) Consider the FK-Ising model on the discretization of the annulus (denoted $\square^n$) between Λ_n and $\Lambda_{\frac{1}{2}n}$, with free boundary conditions. Then

$$\liminf_{n\to\infty} \mathbb{P}^{\mathrm{free}}_{\square^n}\big[\text{ there exists a wired circuit in } \square^n\,\big] \;\geq\; p_0.$$

In particular, it is not required that the successive boxes exhaust the same infinite grids, simply that they have the same $\kappa < 1$ Lipschitz constant.

In order to apply the aforementioned strategy, one should first ensure the possibility of constructing a *proper* s-embedding associated to the abstract weighted graph (G,x), with faces of $\Lambda(G)$ delimited by straight segments and no overlaps. The existence of proper s-embeddings associated to any weighted finite graph G **always holds**, without any particular boundary requirement (see Section 5.1), and it can even be constructed using an *explicit algorithm* coming from [32]. For infinite grids, it is still an open question whether one can find a proper full plane picture in the generic case, and this often requires finding a clever solution to the propagation equation (see the brief discussion at the end of Section 5.1 on a natural condition on the behavior at infinity of solutions to the propagation equation that lead to proper pictures, following [12, Appendix]). We highlight that among the consequences of the current paper, one obtains (see Section 5.1 for a detailed discussions):

- An alternative derivation of the RSW property for the FK-Ising model on critical Z-invariant isoradial lattices as in [14]. Our result extends beyond the scope of the paper of Chelkak and Smirnov, as it allows to replace the bounded angle property by the assumption $\textsc{Exp-Fat}(\delta)$. This replacement allows in particular to rederive the RSW property for the FK representation of the quantum Ising model [20, Section 5] in a more brief manner.
- An alternative derivation of the RSW property for the *massive* Z-invariant model on isoradial grids as in [41], using the re-embedding procedure of [11, Section 3.3]. On the square lattice, this follows directly from the re-embedding procedure as a Layered model presented in Section 5.1.
- An alternative derivation of the RSW property for doubly-periodic graphs given in [5]. In particular, there is no need to use a doubly-periodic canonical embedding to deduce the Theorems 1.1 and 1.2 here. More generally

our results apply to 'flat' origami functions, including circle-patterns of Lis with bounded angles [33] already treated in [5].

- The new derivation of the RSW property for the FK-Ising model on circle patterns introduced in [33], replacing the bounded angle property by the EXP-FAT(δ) assumption (the limiting origami map in this setup is automatically 0). In particular, it is possible apply our result to finite pieces of some random triangulations coming from the discrete mating-of-trees model of Duplantier, Gwynne, Miller and Sheffied [22, 26], and decorate that random graph with Ising weights naturally attached to the associated circle packing. In [25], it was proven that this random map model has no large circles in bounded regions with high probability, and this, together with slightly more refined estimates on the typical number of vertices, fits our framework.
- The derivation of the RSW property for tilings of the plane by tangential quadrilaterals (e.g. the construction of IC nets made by Akopyan and Bobenko [1]) with an origami map whose Lipschitz constant is asymptotically smaller than 1 (see e.g. the zig-zag layered model [10]). In particular, we present in Section 5.1 how to use a pair of discretized s-holomorphic functions to construct starting from an s-embedding new critical lattices with different weights. This method gives a rather simple way to construct many new critical lattices out of already existing ones, via a discrete Weierstrass parametrization of the space-like surface $(z, \mathcal{Q}(z))$, following [11, Section 3.3].

We hope our result motivates research regarding the construction of additional concrete examples.

To prove Theorem 1.1, we use the flexibility of the s-embeddings setup in order to extend the discretization of a well chosen rectangle in $\mathcal{S}^\delta$ and paste it to a piece of the square lattice (see Figure 6 in section 4). Once this extension is done, the proof goes by contradiction, assuming Theorem 1.1 and finding an inconsistency between the boundary behavior of discrete observables and the continuous counterparts. Adding those pieces of the square lattice heavily simplifies the boundary analysis and provides a more digestable proof of the aforementioned inconsistency.

1.4. **Novelties of the paper, related works and open questions.** This article provides a general framework that we hope will open up a path to generalize already known results to new graph settings, and already allows to construct a fair share of new 'critical' Ising models, e.g. in its most simple case using tilings of the plane made out of tangential quadrilaterals coming from a pair of discrete s-holomorphic functions. In all previously known setups, the symmetries, the integrability, the bounded number of neighbors and the finite energy property play a key role. We bypass this difficulty using the flexibility of s-embeddings framework. This idea to paste a piece of an already understood grid is new and relates to the fact that boundary to boundary connection probabilities of the FK model can be studied in bigger domains, modulo the fact that the (abstract) layers where we 'weld' the two graphs do not completely break connectivity.

From our perspective, this allows to formulate some notion of criticality for the Ising model on a generic planar graph, following [5, (**II**) in Section 1.5]:

Which are the spectral properties of the propagation operator (2.6) (or the associated Kac-Ward matrix) that imply the existence of a complex valued solution $\mathcal{X}$ to the propagation equation such that the associated s-embedding $\mathcal{S}_{\mathcal{X}}$ satisfies $\mathrm{Lip}(\kappa,\delta)$ for a large enough δ?

This question has been investigated in a periodic setup in a joint work with Chelkak and Hongler (see [10, Section 5]) and is related there to spectral characteristics of the operator near the bottom of its spectrum. In that article, one even recovers features of the canonical realization in the Euclidean plane in the coefficients of the expansion of the integrated density of states near $\lambda = 0$ (see [10, Equation (5.8)]). Generalizing this understanding would allow to reformulate exactly the present notion of criticality from the Kac-Ward operator perspective.

We expect that off-critical models lead to embeddings with an optimal Lipschitz contant being one, as discussed in Section 5.2 concerning near critical and off-critical models. One can also hope to prove the convergence of crossing probabilities by expressing them in the four points setup via some quasi-conformal uniformization in a fashion similar to the critical or near critical case [41, Section 5]. This approach is being investigated in a article in preparation with Park [35]. More generally, we view the current paper as the first step towards the proof of existence of a scaling limit for the Ising model on general s-embeddings. The associated continuous limit and its relation to the Lorentz geometry and quasi-conformal maps (see [12] and [5, Section 2.7]) will be carried out jointly with Park [35, 36] following the root started in [34, Chapter 6]. In particular, our result classically ensures precompactness of FK-Interfaces on general s-embeddings satisfying $\mathrm{Lip}(\kappa,\delta)$ and $\mathrm{Exp\text{-}Fat}(\delta)$ (see e.g. [31]).

From our perspective, the most interesting question is to use the meta-framework developed here to attack the question of crossing probabilities on random planar maps (with some coupling constants to be properly chosen) or on $\mathbb{Z}^2$ with random coupling constants. Finally, another interesting line of research would be to extend the strategy of [21] to prove crossing estimates which are uniform with respect to local structure of the lattice and boundary conditions, by bootstrapping Theorem 1.2 for $\mathrm{Unif}(\delta)$ type grids. We are not able to handle such problem as for now, since a similar strategy requires a comparison between primal and dual arm exponents in the half-plane, which is not straightforward additional symmetries.

Acknowledgements. The author is deeply indebted to Dmitry Chelkak for introducing him to this field, for constant support and careful reading of earlier versions of this manuscript. We are also grateful to Sung-Chul Park for valuable discussions and carefully reading earlier versions of this manuscript as well as Mikhail Basok for crucial help regarding Beltrami equations. An earlier version of this text was part of the thesis of the author, completed when he was a student at Ecole Normale Supérieure. R.M. is grateful for the support of the institution. The author is also grateful to Niklas Affoter, Nikolai Bobenko, Cédric Boutillier, Béatrice de Tilière, Trishen Gunaratnam, Konstantin Izyurov, Emmanuel Kammerer, Dmitrii Krachun, Ioan Manolescu, Seginus Mowlavi, Mendes Oulamara, Christophoros Panagiotis, Romain Panis, Sanjay Ramassamy, Stanislav Smirnov and Yijun Wan for useful discussions and helpful remarks. This research is funded by Swiss National Science Foundation and the NCCR SwissMAP.

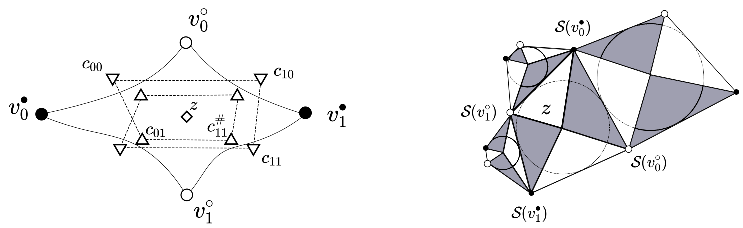

FIGURE 2. (Left) Local notations of a graph given an arbitrary embedding of a planar graph for a quad $z\diamondsuit(G)$. Vertices of the primal graph $G^\bullet$ are drawn as black dots, vertices of the dual graph G° (which correspond to faces of $G^\bullet$) are drawn as white dots, and corners (which correspond to edges of the bipartite graph $G^\bullet \cup G^\circ$) are drawn as triangles. We present here a piece of the *double cover* of the corner graph that branches around z. Neighboring corners in the double cover are linked with dashes. (Right) A small piece of the associated face in an s-embedding, together with neighboring faces. Each face in this proper s-embedding is a tangential quadrilateral, not necessarily convex. The bipartite splinting of each face of $\Lambda(G)$ in four triangles corresponds to the dimer identification under the s/t-embeddings correspondence (see [5, Section 2.3] for more details.)

2. DEFINITIONS AND CRASH INTRODUCTION TO THE S-EMBEDDINGS FORMALISM

We recall in the section the construction of s-embeddings introduced in [5, Section 3] and the regularity theory of s-holomorphic functions, both based upon a complexification procedure of the Kadanoff-Ceva formalism. The notations we use in this paper follow exactly those of [5] and agree with those of [7, Section 3] and [6]. We proceed below without giving any proof, referring to [5, Section 2] for more details. The overall idea of the construction is to start with an abstract weighted planar graph and construct an embedding where discrete complex analysis techniques are available.

2.1. **Notation and Kadanoff–Ceva formalism.** We fix G a planar graph (allowing multi-edges and vertices of degree two but forbidding loops and vertices of degree one) with the combinatorics of the plane or of the sphere, considered up to homeomorphisms preserving cyclic ordering of edges around each vertex. In the sphere case, we prescribe one of the faces of G and call it the outer face of G. We denote $G = G^\bullet$ the original graph whose vertices are denoted by $v^\bullet \in G^\bullet$ and G° its dual, whose vertices are denoted by $v^\circ \in G^\circ$. The faces of the bipartite graph $\Lambda(G) := G^\circ \cup G^\bullet$ (with natural incidence relation) are in bijection with edges of G. We also denote $\diamondsuit(G)$ the graph dual to $\Lambda(G)$, whose vertices are often denoted by $z \in \diamondsuit(G)$ and called quads. Finally, we denote by $\Upsilon(G)$ the medial graph of $\Lambda(G)$. The vertices of $\Upsilon(G)$ are in bijection with edges $(v^\bullet v^\circ)$ of $\Lambda(G)$. The vertices $c \in \Upsilon(G)$ are called corners of G. To make the formalism consistent, one needs to consider several double covers of $\Upsilon(G)$, see e.g. [38, Fig. 27] or [5, Fig 3.A] for relevant pictures. Denote by $\Upsilon^\times(G)$ the double cover that branches over all faces of $\Upsilon(G)$ (each $v^\bullet \in G^\bullet, v^\circ \in G^\circ, z \in \diamondsuit(G)$). When G is finite, this definition of the double cover remains meaningful as $\#(G^\bullet)+\#(G^\circ)+\#(\diamondsuit(G))$ is even due to the Euler theorem. Given $\varpi = \{v_1^\bullet, \dots, v_m^\bullet, v_1^\circ, \dots, v_n^\circ\} \subset \Lambda(G)$ where n, m are even, denote by $\Upsilon^\times_\varpi(G)$ the double cover of $\Upsilon(G)$ branching over all its faces except those ϖ, and by $\Upsilon_\varpi(G)$ the double cover of $\Upsilon(G)$ branching only over those ϖ. We call a *spinor* a function defined on one of the aforementioned double covers whose value at two different lifts of the same corner differ by a multiplicative factor -1.

In this paper, we consider the Ising model on faces of G, including the outer face in the disc case, i.e. the model assigns ± 1 random variables to vertices of G° with a partition function given by (1.1). The domain walls representation [7, Section 1.2] (also called low-temperature expansion) assigns a spin configuration $\sigma : G^\circ \to \{\pm 1\}$ to a subset C of edges of G that separates spins of opposite signs; this expansion is a 2-to-1 mapping from spin configurations onto the set $\mathcal{E}(G)$ of even subgraphs of G, depending on the value of the spin of the outer face.

Given $v_1^\circ, \dots, v_n^\circ \in G^\circ$ where n is even, fix a subgraph $\gamma^\circ = \gamma_{[v_1^\circ,\dots,v_n^\circ]} \subset G^\circ$ with odd degree at vertices of $v_1^\circ, \dots, v_n^\circ$ and even degree at all other vertices of G°. On can represent such configuration as a collection of paths on G° linking pairwise vertices of $v_1^\circ, \dots, v_n^\circ$. Denote

$$x_{[v_1^\circ,\dots,v_n^\circ]}(e) \;:=\; (-1)^{e\cdot\gamma_{[v_1^\circ,\dots,v_n^\circ]}}\, x(e), \quad e \in E(G),$$

where $e \cdot \gamma = 0$ if e doesn't cross γ and $e \cdot \gamma = 1$ otherwise. One can see that

$$\mathbb{E}\big[\sigma_{v_1^\circ} \dots \sigma_{v_n^\circ}\big] \;=\; x_{[v_1^\circ,\dots,v_n^\circ]}(\mathcal{E}(G))/x(\mathcal{E}(G)), \tag{2.1}$$

where $x(\mathcal{E}(G)) := \sum_{c\in\mathcal{E}(G)} x(C)$, $x(C) := \prod_{e\in C} x(e)$, and similarly for $x_{[v_1^\circ,\dots,v_n^\circ]}$.

For m even and $v_1^\bullet, \dots, v_m^\bullet \in G^\bullet$, fix again subgraph $\gamma^\bullet = \gamma^{[v_1^\bullet,\dots,v_m^\bullet]} \subset G^\bullet$ with even degree at all vertices of $G^\bullet$ except those of $v_1^\bullet, \dots, v_m^\bullet$. Following the formalism of Kadanoff and Ceva [30], one changes the signs of the interaction constants $J_e \mapsto -J_e$ on edges $e \in \gamma^\bullet$. This inversion (which is equivalent to replacing $x(e)$ by $x(e)^{-1}$ along the edges of $\gamma^\bullet$) makes the model anti-ferromagnetic near $\gamma^\bullet$, favoring locally configurations with nonaligned spins, and is denoted by the notation $\mu_{v_1^\bullet} \dots \mu_{v_m^\bullet}$. More precisely, we introduce the random variable (which depends on the choice of $\gamma^\bullet$)

$$\mu_{v_1^\bullet} \dots \mu_{v_m^\bullet} \;:=\; \exp\big[-2\beta \textstyle\sum_{e\in\gamma^{[v_1^\bullet,\dots,v_m^\bullet]}} J_e \sigma_{v_-^\circ(e)} \sigma_{v_+^\circ(e)} \big],$$

the domain walls representation shows that (e.g. [7, Propositon 1.3])

$$\mathbb{E}\big[\mu_{v_1^\bullet} \dots \mu_{v_m^\bullet}\big] \;=\; x(\mathcal{E}^{[v_1^\bullet,\dots,v_m^\bullet]}(G))/x(\mathcal{E}(G)), \tag{2.2}$$

where $\mathcal{E}^{[v_1^\bullet,\dots,v_m^\bullet]}$ denotes the set of subgraphs of G with even degrees at all vertices except at those of $v_1^\bullet, \dots, v_m^\bullet$ which have odd degrees at the last mentioned. Let us mention that when taking expectations in (2.2), the result does not depend on the choice of the path $\gamma^\bullet$. One can also generalize (2.1) and (2.2) mixing the presence of spins and disorder, which reads as (e.g. [7, Propositon 3.3])

$$\mathbb{E}\big[\mu_{v_1^\bullet} \dots \mu_{v_m^\bullet} \sigma_{v_1^\circ} \dots \sigma_{v_n^\circ}\big] \;=\; x_{[v_1^\circ,\dots,v_n^\circ]}(\mathcal{E}^{[v_1^\bullet,\dots,v_m^\bullet]}(G))/x(\mathcal{E}(G)), \tag{2.3}$$

where $\mu_{v_1^\bullet} \dots \mu_{v_m^\bullet}$ are understood as above. The *sign* of this last expression does depends on the parity number of intersections between γ° and $\gamma^\bullet$. There is no canonical way to chose of that sign in (2.3) staying on the Cartesian product

$(G^\bullet)^{\times m}\times(G^\circ)^{\times n}$. However, one can first fix $\mathcal{S}:\Lambda(G)\to\mathbb{C}$ to be an arbitrarily chosen embedding of G, and consider a natural double cover of this Cartesian product, whose branching structure is the one of the spinor $[\prod_{p=1}^m\prod_{q=1}^n(\mathcal{S}(v_p^\bullet)-\mathcal{S}(v_q^\circ))]^{1/2}$. As discussed in great details in [9, Section 2.2], the expectations of the form (2.3) can be seen as spinors on the above described double cover of $(G^\bullet)^{\times m}\times(G^\circ)^{\times n}$. When treating mixed correlation of the type (2.3), an extension of the usual Kramers-Wannier duality (again [7, Propositon 3.3]) implies that the roles played by the graphs $G^\bullet$ and G° are now equivalent.

We are now going to consider special correlators of the form (2.3), in the case where one of the disorders $v^\bullet(c)\in G^\bullet$ and one of the spins $v^\circ(c)\in G^\circ$, are neighbors in $\Lambda(G)$, and separated by a corner $c\in\Upsilon(G)$. In that case, one can *formally* denote the fermion at the corner c by

$$\chi_c:=\mu_{v^\bullet(c)}\sigma_{v^\circ(c)}, \tag{2.4}$$

Using equation (2.3), one can then define the Kadanoff–Ceva *fermionic observables* by

$$X_\varpi(c):=\mathbb{E}[\,\chi_c\mu_{v_1^\bullet}\dots\mu_{v_{m-1}^\bullet}\sigma_{v_1^\circ}\dots\sigma_{v_{n-1}^\circ}]. \tag{2.5}$$

This definition is purely abstract and doesn't require an embedding. Following the above remarks, one can see that $X_\varpi(c)$ is a priori defined up to the sign, but the definition becomes fully legitimate when passing to $\Upsilon_\varpi^\times(G)$. Around a quad $z=(v_0^\bullet,v_0^\circ,v_1^\bullet,v_1^\circ)$ whose vertices are listed in the counterclockwise order (see [5, Figure 3.A] for the notation), that Kadanoff–Ceva fermionic observables satisfy a local linear propagation equation, whose coefficients are determined by the Ising interaction parameters. This propagation equation appeared in the works of [16], [42] and [38, Section 4.3]) and reads as follows:

$$X(c_{pq})=X(c_{p,1-q})\cos\theta_z+X(c_{1-p,q})\sin\theta_z, \tag{2.6}$$

where the corner c_{pq} is identified as $c_{pq}=(v_p^\bullet v_q^\circ)$, the lifts of c_{pq}, $c_{p,1-q}$ and of $c_{1-p,q}$ to $\Upsilon_\varpi^\times(G)$ are neighbors, and the angle θ_z corresponds to the abstract parametrization (1.2) of the edge of $G^\bullet$ which corresponds to the quad centered at z. One can easily show that solutions to (2.6) are automatically spinors on $\Upsilon_\varpi^\times(G)$.

We conclude this reminder on Kadanoff-Ceva correlators by recalling the definition of the spinor η_c, that is a special solution (i.e. with some geometrical interpretation) to the propagation equation (2.6) on isoradial grids. Given any embedding $\mathcal{S}:\Lambda(G)\to\mathbb{C}$ of $\Lambda(G)$ into the complex plane, denote following [14]

$$\eta_c:=\varsigma\cdot\exp\big[-\tfrac{i}{2}\arg(\mathcal{S}(v^\bullet(c))-\mathcal{S}(v^\circ(c)))\big],\qquad \varsigma:=e^{i\frac{\pi}{4}}, \tag{2.7}$$

where the prefactor $\varsigma=e^{i\frac{\pi}{4}}$ is chosen for convenience reasons. As explained previously, one can once again avoid the sign ambiguity in the definition (2.7) by passing to the double cover $\Upsilon^\times(G)$, understanding the products $\eta_cX_\varpi(c):\Upsilon_\varpi(G)\to\mathbb{C}$ as defined on the double cover $\Upsilon_\varpi(G)$ that only branches over ϖ. Note that below, we use the notation (2.7) even when $\mathcal{S}$ is not isoradial.

2.2. **Definition of s-embeddings.** We present now in a concise way the explicit embedding procedure introduced in [6, Section 6] and then developed in great details in [5]. We start by recalling the concrete definition of an s-embedding given in [5, Definition 2.1], using the Kadanoff-Ceva formalism recalled in Section 2.1. The general idea is to use a solution to (2.6) to construct the picture.

Definition 2.1. Let (G, x) be a weighted planar graph with the combinatorics of the plane and $\mathcal{X} : \Upsilon^\times(G) \to \mathbb{C}$ a solution to the propagation equation (2.6). We say that $\mathcal{S} = \mathcal{S}_\mathcal{X} : \Lambda(G) \to \mathbb{C}$ is an s-embedding of (G, x) associated to $\mathcal{X}$ if for each $c \in \Upsilon^\times(G)$, we have

$$\mathcal{S}(v^\bullet(c)) - \mathcal{S}(v^\circ(c)) = (\mathcal{X}(c))^2. \tag{2.8}$$

For $z \in \diamondsuit(G)$, denote by $\mathcal{S}^\diamond(z) \subset \mathbb{C}$ the quadrilateral whose vertices are points $\mathcal{S}(v_0^\bullet(z))$, $\mathcal{S}(v_0^\circ(z))$, $\mathcal{S}(v_1^\bullet(z))$, $\mathcal{S}(v_1^\circ(z))$. The s-embedding $\mathcal{S}$ is said to be *proper* if the quadrilaterals $\mathcal{S}^\diamond(z) = (\mathcal{S}(v_0^\bullet(z))\mathcal{S}(v_0^\circ(z))\mathcal{S}(v_1^\bullet(z))\mathcal{S}(v_1^\circ(z)))$ do not overlap with each other, and is said to be non-degenerate if no quads $\mathcal{S}^\diamond(z)$ degenerates to a segment. In particular, the convexity of $\mathcal{S}^\diamond(z)$ is not required.

Let us make clear that it is not at all automatic that, given any solution $\mathcal{X}$ to the propagation equation, the associated picture $\mathcal{S}_\mathcal{X}$ is proper, and finding a solution to (2.6) that leads to a non-degenerate proper picture is a non-trivial step. One can also extend the definition of $\mathcal{S}$ to the set $\diamondsuit(G)$ by setting [5, Equation (2.5)]

$$\begin{aligned} \mathcal{S}(v_p^\bullet(z)) - \mathcal{S}(z) &:= \mathcal{X}(c_{p0})\mathcal{X}(c_{p1}) \cos\theta_z, \\ \mathcal{S}(v_q^\circ(z)) - \mathcal{S}(z) &:= -\mathcal{X}(c_{0q})\mathcal{X}(c_{1q}) \sin\theta_z, \end{aligned} \tag{2.9}$$

where c_{p0} and c_{p1} (respectively, c_{0q} and c_{1q}) are neighbors on $\Upsilon^\times(G)$. The propagation equation (2.6) implies directly the consistency of both definitions (2.8) and (2.9).

The second object of crucial relevance in the s-embeddings framework is the so called origami map. It is the large scale properties of the origami map that will indicate whether one can interpret the abstract graph to a (near)-critical system or not. We recall now the definition [5, Definition 2.2] which can also be found (with appropriate Ising/dimers identifications) in [32, 13].

Definition 2.2. Given $\mathcal{S} = \mathcal{S}_\mathcal{X}$, one can construct the *origami* function denoted by $\mathcal{Q} = \mathcal{Q}_\mathcal{X} : \Lambda(G) \to \mathbb{R}$, as a real valued function (defined up to a global additive constant) by declaring its increments between $v^\bullet(c)$ and $v^\circ(c)$ to be

$$\mathcal{Q}(v^\bullet(c)) - \mathcal{Q}(v^\circ(c)) \;:=\; |\mathcal{X}(c)|^2 \;=\; |\mathcal{S}(v^\bullet(c)) - \mathcal{S}(v^\circ(c))| \,. \tag{2.10}$$

Once again, the propagation equation (2.6) implies directly the consistency of the definition (2.2). In words, this implies that alternates sum of edge-length around a quad vanishes. This ensures the image $\mathcal{S}^\diamond(z)$ of a quad into the complex plane is a quadrilateral tangential to a circle centered at the point $\mathcal{S}(z)$ given by (2.9). The point $\mathcal{S}(z)$ is the intersection point of the four bisectors of the angles of the tangential quadrilateral $\mathcal{S}^\diamond(z)$. We denote by r_z the radius of the circle, which can be recovered from the values of χ, using e.g. [5, Equation (2.7)]. If one denotes ϕ_{vz} the half-angle of the quad $\mathcal{S}^\diamond(z)$ at $\mathcal{S}(v)$, the Ising weight θ_z (in the parametretrization (1.2)) can be recovered from the angles in $\mathcal{S}$ plane using the formula [5, Equation (2.8)]

$$\tan\theta_z \;=\; \left(\frac{\sin\phi_{v_0^\bullet z}\sin\phi_{v_1^\bullet z}}{\sin\phi_{v_0^\circ z}\sin\phi_{v_1^\circ z}}\right)^{1/2}. \tag{2.11}$$

As explained in [5, Section 2.3] (see also [32, Section 7]), one can see that if $\mathcal{S}$ is proper and non-degenerate, the map $\mathcal{S} : \Lambda(G) \cup \diamondsuit(G) \to \mathbb{C}$ is a *t-embedding* $\mathcal{T}$ and $\eta_{c^\bullet} = \eta_{c^\circ} := \bar{\varsigma}\eta_c$ is an origami square root (see [13, Definition 2.4]) of $\mathcal{T}$. This identification allows (e.g. [13, Appendix]) to extend the origami map $\mathcal{Q}$ into a piece-wise linear way to the *entire* plane (taking complex values inside the faces of the t-embedding), and not only on edges of $\Lambda(G)$.

2.3. **S-holomorphic functions and associated functions H_F and $I_{\mathbb{C}}$.** We recall now the central notion of *s-holomorphic functions* (generalized to s-embeddings in [5]), introduced first for the critical square grid by Smirnov [43, Definition 3.1] and generalized to the isoradial context by Chelkak and Smirnov in [14, Definition 3.1] (it is in the latter paper that this name was coined). That notion is at the heart of the use of of discrete complex analysis techniques to study the Ising model. Under the link (briefly mentioned above) between s and t-embeddings, the s-holomorphic functions are special cases of *t-holomorphic* functions introduced in the dimers context in [13, Definition 3.2], which allows to use the regularity theory proved in that later paper. We recall now the general definition on s-holomorphic functions, given in [5, Definition 2.4].

Definition 2.3. A function F defined on a subset of $\diamondsuit(G)$ is called s-holomorphic if

$$\Pr[F(z),\eta_c\mathbb{R}] = \Pr[F(z'),\eta_c\mathbb{R}] \tag{2.12}$$

for each pair of quads $z,z'\in\diamondsuit(G)$ adjacent to the same edge $(v^\circ(c)v^\bullet(c))$ in $\mathcal{S}$.

The next proposition generalizes beyond the isoradial setup (e.g. [14, Lemma 3.4]) the (bijective) link between real valued solutions to the propagation equation (2.6) and s-holomorphic functions. This link was already presented in [5, Proposition 2.5] and in [13, Appendix].

Proposition 2.4. *Let $\mathcal{S}=\mathcal{S}_{\mathcal{X}}$ be a proper s-embedding and F an s-holomorphic on a subset of $\diamondsuit(G)$. Then, the spinor X defined at corners $c\in\Upsilon^\times(G)$ belonging to the face $z\in\diamondsuit(G)$ by*

$$\begin{aligned} X(c) &:= |\mathcal{S}(v^\bullet(c))-\mathcal{S}(v^\circ(c))|^{\frac{1}{2}}\cdot\mathrm{Re}[\overline{\eta}_c F(z)] \\ &= \mathrm{Re}[\overline{\varsigma}\mathcal{X}(c)\cdot F(z)] \;=\; \overline{\varsigma}\mathcal{X}(c)\cdot\Pr F(z)\eta_c\mathbb{R} \end{aligned} \tag{2.13}$$

satisfies the propagation equation (2.6) *around z.*

Conversely for $X:\Upsilon^\times(G)\to\mathbb{R}$ a unique real valued solution to (2.6)*, there exists a s-holomorphic function F such that* (2.13) *is fulfilled.*

When F and X are linked by (2.13), one can reconstruct the value of F at $z\in\diamondsuit$ from the values of X at any pair of corners $c_{pq}(z)\in\Upsilon^\times(G)$, e.g. [5, Corollary 2.6]

$$F(z) \;=\; -i\varsigma\cdot\frac{\overline{\mathcal{X}(c_{01}(z))}\,X(c_{10}(z))-\overline{\mathcal{X}(c_{10}(z))}\,X(c_{01}(z))}{\mathrm{Im}[\,\overline{\mathcal{X}(c_{01}(z))}\,\mathcal{X}(c_{10}(z))}. \tag{2.14}$$

To study the regularity of s-holomorphic functions as well as the local behavior of their scaling limit, one uses their 'integral' while one uses generalization of the 'integral' of the imaginary part of their square introduced by Smirnov in [43] to derive their boundary behavior. The former is heavily studied in [13, Proposition 6.15] and will be useful deriving local regularity theory for discrete functions as well as the local equation satisfied by subsequential limits in continuum, while the latter was introduced by Smirnov in [43] on the critical square grid and has since been exploited in several different contexts to identify the scaling limit of fermionic observables. We start with the integral $I_{\mathbb{C}}$ of an s-holomorphic function. In [5, Section 2.5 of], s-holomorphic functions are described as gradients of harmonic functions on the associated S-graphs, specializing in the Ising context the technology developed in [13, Section 4.2] for t-holomorphic functions. Given an s-holomorphic function F on $\diamondsuit(G)$, one can define in the continuum plane (up to a global additive constant) [5, Section 2.3]

$$I_{\mathbb{C}}[F] := \int \left(\overline{\varsigma} F d\mathcal{S} + \varsigma \overline{F} d\mathcal{Q}\right) \tag{2.15}$$

Let $v^\bullet_{1,2}, v^\circ_{1,2}$ be vertices of the quad $z \in \diamondsuit(G)$. Then one has for $\star \in \{\bullet, \circ\}$

$$I_{\mathbb{C}}[F](v_2^\star) - I_{\mathbb{C}}[F](v_1^\star) = \overline{\varsigma} F(z)[\mathcal{S}(v_2^\star) - \mathcal{S}(v_1^\star)] + \varsigma \overline{F(z)}[\mathcal{Q}(v_2^\star) - \mathcal{Q}(v_1^\star)]. \tag{2.16}$$

As for the imaginary part of the primitive of the square H, we start by recalling first its combinatorial definition (i.e. which doesn't require any particular embedding into the plane) for spinors on $\Upsilon^\times(G)$ satisfying (2.6). Afterwards, we precise its analytic interpretation in the context of s-embeddings. This definition, which represents a generalisation of the original work of Smirnov, can be found in the following form in [5, Definition 2.8].

Definition 2.5. Given X a spinor on $\Upsilon^\times(G)$ satisfying (2.6), one defines the function H_X up to a global additive constant on $\Lambda(G) \cup \diamondsuit(G)$ by setting

$$\begin{array}{rcll} H_X(v_p^\bullet(z)) - H_X(z) & := & X(c_{p0}(z))X(c_{p1}(z))\cos\theta_z, & p = 0, 1, \\ H_X(v_q^\circ(z)) - H_X(z) & := & -X(c_{0q}(z))X(c_{1q}(z))\sin\theta_z, & q = 0, 1, \\ H_X(v_p^\bullet(z)) - H_X(v_q^\circ(z)) & := & (X(c_{pq}(z)))^2, & \end{array} \tag{2.17}$$

similarly to (2.8) and (2.9).

The consistency of the above definition follows once again from the propagation equation (2.6). Passing to an s-embedding $\mathcal{S}$ of (G, x), one can use the correspondence between X and F recalled in Proposition 2.4 to interpret H_X via the s-holomorphic function F associated to X. More precisely, it is possible to define [5, Equation (2.17)]

$$H_F := \int \mathrm{Re}(\overline{\varsigma}^2 F^2 d\mathcal{S} + |F|^2 d\mathcal{Q}) = \int (\mathrm{Im}(F^2 d\mathcal{S}) + \mathrm{Re}(|F|^2 d\mathcal{Q})), \tag{2.18}$$

on $\Lambda(G) \cup \diamondsuit(G)$. The function H_F extends linearly to a piece-wise affine function on each faces of the t-embedding $\mathcal{T} = \mathcal{S}$ (but not on each face of $\diamondsuit(G)$ as each face of $\mathcal{T}$ has its own origami square root $d\mathcal{Q}$), at least if one stays in the bulk of G (see [13, Proposition 3.10]). The next lemma links the definitions (2.17) and (2.18), proving that they are in fact the *same* function.

Lemma 2.6. *[5, Lemma 2.9] Let F be defined $\diamondsuit(G)$ and X be defined on $\Upsilon^\times(G)$ related by the identity* (2.13). *Then, the functions H_F and H_X coincide up to a global additive constant.*

If $\mathcal{S}$ is an isoradial grid, the origami map $\mathcal{Q}$ is constant on both $G^\bullet$ and G° (as all the edges of any quad $\mathcal{S}^\diamond(z)$ are all of the same length), thus H_F is the primitive of $\mathrm{Im}[F^2 d\mathcal{S}]$, recovering the original definition given in [14, Section 3.3]. We now recall the comparison principle for functions $H_F = H_X$ associated with s-holomorphic functions. This statement is due to Park and can be found in [5, Proposition 2.11]. In particular, when one of the observables in the following proposition is identically 0, this proposition becomes a maximum principle.

Proposition 2.7. *Let spinors $X, Y : \Upsilon^\times(G) \to \mathbb{R}$ both satisfy the propagation equation* (2.6) *and the associated functions $H_X, H_Y : \Lambda(G) \cup \diamondsuit(G) \to \mathbb{R}$ be defined via* (2.17)*. Then, the difference $H_X - H_Y$ cannot have an extremum at an interior vertex of its domain of definition.*

In particular if H_X is bounded at the boundary of a domain (which is trivially the case for the observables defined in Section 3), then $H_X = H_F$ is bounded everywhere in the domain.

2.4. **Regularity theory for s-holomorphic functions.** In this short subsection we recall in a concise way the regularity theory of s-holomorphic functions, which is developed in [5, Section 2.6], adapting to the Ising context results coming from [13, Section 6]. Our proof of crossing estimates is based on a contradiction between the discrete behavior and its scaling limit, and thus we need to explain how to extract sub-sequential limits from discrete observables. We start by recalling that regularity theory of s-holomorphic functions requires adding one (mild) geometrical constraints on potential local degeneracies of the embedding, following [13, Assumption 1.2]. In that case, an s-holomorphic function F satisfies a standard Harnack-type estimate that controls $|F|^2$ via the gradient of the function H_F.

Corollary 2.8. *[5, Corollary 2.20] Let $\kappa < 1$ and a sequence of s-embeddings $\mathcal{S}^\delta$ satisfying* $\textsc{Lip}(\kappa,\delta)$ *and* $\textsc{Exp-Fat}(\delta)$ *in a disc $U = B(u, r)$. Assume that F^δ is an s-holomorphic function on $\mathcal{S}^\delta$ and that $\max_{v:\mathcal{S}(v)\in U} |H_{F^\delta}(v)| \le M$ for all δ. Then, the following uniform (as $\delta \to 0$) estimate holds:*

$$|F^\delta(z)|^2 = O(r^{-1}M) \quad \text{if} \ \ \mathcal{S}^\delta(z) \in B(u, \tfrac{1}{2}r). \tag{2.19}$$

In particular, the functions H_{F^δ} are uniformly Lipschitz on compact subsets of U.

Remark 2.9. Under the assumptions of Corollary 2.8, [5, Remark 2.11] also ensures that the functions F^δ form a precompact family in the topology of the uniform convergence on compacts of $B(u, r)$ as $\delta \to 0$. Indeed, those functions are uniformly bounded and β-Hölder (see [5, Theorem 2.18]) on scales above $\mathrm{cst}(\kappa) \cdot \delta$. Let us also remark that, in the case where the functions F^δ are constructed out of Kadanoff-Ceva correlators, it is possible to weaken the assumptions of Corollary 2.8 in the approximation of a fixed macroscopic domain, replacing the assumption $\textsc{Exp-Fat}(\delta)$by simply assuming the existence of a positive function $o_{\delta\to 0}(1)$ such that *all* boundary quads approximating that domain have a radius $r_z \ge \exp(o_{\delta\to 0}(1)\delta^{-1})$. Indeed, in that new scenario, that second alternative of [5, Theorem 2.18] stating the exponential blow up (in δ^{-1}) of $|F|^2$ is not possible. Indeed, the projections $\mathrm{Re}[F]$ and $\mathrm{Im}[F]$ are martingales for some random walk in the appropriate S-graphs and thus satisfy the maximum and minimum principle. On the other hand, at the boundary quads, the formula (2.14) ensures that $|F| = O(\exp(o_{\delta\to 0}(1)\delta^{-1}))$, thus forcing the first alternative of [5, Theorem 2.18] to hold, which is exactly Corollary 2.8.

2.5. **Subsequential limits of s-holomorphic functions.** We discuss now the behavior of subsequential limits of s-holomorphic functions, under the general hypothesis $\textsc{Lip}(\kappa,\delta)$, following [5, Section 2.7]. In what follows, we work with proper s-embeddings $\mathcal{S}^\delta$ all satisfying the assumption $\textsc{Lip}(\kappa,\delta)$ as $\delta \to 0$ *for the same constant* $\kappa < 1$, such that their respective images cover a given ball $U = B(u, r) \subset \mathbb{C}$. As the functions $\mathcal{Q}^\delta$ all are κ-lipschitz above scale $\asymp \delta$ and are defined up to an additive constant, there exist a sub-sequence $\delta_k \to 0$ and a κ-Lipschitz function $\vartheta : U \to \mathbb{R}$ such that uniformly on compacts of U,

$$\mathcal{Q}^{\delta_k} \circ (\mathcal{S}^{\delta_k})^{-1} \to \vartheta. \tag{2.20}$$

Assuming now we are in the setup of Corollary 2.8 and that (2.20) holds, consider $f : U \to \mathbb{C}$ a subsequential limit of s-holomorphic functions F^δ on $\mathcal{S}^\delta$. Then following [5, Proposition 2.21] and setting $\varsigma = e^{i\frac{\pi}{4}}$ as in (2.7), the differential form $\frac{1}{2}(\bar{\varsigma} f dz + \varsigma \overline{f} d\vartheta)$ is closed. This comes as a natural counterpart of the consistency in the definition of the primitive $I_{\mathbb{C}}$ in (2.15) (as contour integrals of discrete functions vanish before passing to the limit). With a consistent choice of additive constants, the associated functions H_{F^δ} also converge uniformly on compact subsets of U to $h := \int (\mathrm{Im}(f^2 dz) + |f|^2 d\vartheta)$.

The previous condition on closeness of $\frac{1}{2}(\bar{\varsigma} f dz + \varsigma \overline{f} d\vartheta)$ is not easily tractable and hard to interpret in terms of the local relation satisfied by f. In [5, Section 2.7], Chelkak provides a nicer description when passing to the conformal parametrization of the an appropriate surface in the Minkowski space $\mathbb{R}^{2,1}$, equipped with the inner product of signature $(2,1)$.

On first recalls that the function ϑ is κ-Lipschitz, thus differentiable almost everywhere. One can then consider (as in [5, Equation (2.26)]) an orientation-preserving *conformal parametrization* of the space-like surface $(z, \vartheta(z))_{z\in U}$, equipped with a positive metric coming from the ambient Minkowski space

$$\mathbb{D} \ni \zeta \;\mapsto\; (z, \vartheta) \in U \times \mathbb{R} \;\subset \mathbb{C} \times \mathbb{R} \;\cong \mathbb{R}^{2+1} \tag{2.21}$$

As noted in [5, below Equation (2.26)], in the case where ϑ is a smooth function, the angles (measured in $\mathbb{R}^{2,1}$) of infinitesimal increments are preserved by the mapping (2.21) if and only if *everywhere* in $\mathbb{D}$, one has [5, Equation (2.27)]

$$z_\zeta \overline{z}_\zeta \;=\; (\vartheta_\zeta)^2 \quad \text{and} \quad |z_\zeta| > |\vartheta_\zeta| \geq |\overline{z}_\zeta|, \tag{2.22}$$

where $z_\zeta := \partial z / \partial \zeta$ (similarly, $\overline{z}_\zeta$ and ϑ_ζ) stands for the usual Wirtinger derivatives.

Without assuming any smoothness assumption on ϑ, one can note that conformal parametrization of (2.22) can be equivalently rewritten as a *quasi-conformal* map $z \mapsto \zeta(z)$ (solution to a Beltrami equation):

$$\zeta_{\bar{z}} = \mu(z)\zeta_z, \tag{2.23}$$

(or in an equivalent way to $z_\zeta = -\overline{\mu(\zeta)} z_\zeta$), with the Beltrami coefficient μ given by the equation

$$\frac{\bar{\mu}}{1+|\mu|^2} = -\frac{\vartheta_z^2}{1-2|\vartheta_z|^2}, \tag{2.24}$$

This equivalence can be seen by plugging the identity $\vartheta_\zeta = \vartheta_z z_\zeta + \vartheta_{\bar{z}} \bar{z}_\zeta$ (using the fact that ϑ is real valued) into the condition (2.22), which rewrites as $-\overline{\mu} = (\vartheta_z - \overline{\mu}\vartheta_{\bar{z}})^2$. Since $\vartheta_{\bar{z}} = \overline{\vartheta_z}$, this justifies the equality (2.24). Moreover the function $z \mapsto \vartheta(z)$ is κ-Lipschitz for some $\kappa < 1$, which proves that $|\vartheta_z| \leq \frac{\kappa}{2}$ and ensures that $|\mu| \leq \mathrm{cst}(\kappa) < 1$ (see [5, Equation (2.30)]). One can now proceed as follows

- Compute the Beltrami coefficient $\mu \in L^\infty$ from the equation (2.24) *almost everywhere*, as ϑ is differentiable almost everywhere for the Lebesgue measure.
- Use the Ahlfors-Bers's measurable Riemann mapping theorem [2, Chapter 5] to solve the Beltrami equation (2.23), constructing a quasi-conformal uniformization $\zeta : U \mapsto \mathbb{D}$ such that (2.22) holds almost everywhere in $\mathbb{D}$.

In the $\zeta \in \mathbb{D}$ parametrization, one can make a convenient change of variables as in [5, Equation (2.28)], by defining the functions

$$\phi(\zeta) := \bar{\varsigma} f(z(\zeta)) \cdot (z_\zeta)^{1/2} + \varsigma \overline{f(z(\zeta))} \cdot (\overline{z}_\zeta)^{1/2} \tag{2.25}$$

Under this change of variables, $I_{\mathbb{C}}[f] := \int \bar{\varsigma} f(z) dz + \varsigma \overline{f(z)} d\vartheta$ reads as

$$g(\zeta) = \int \bar{\varsigma}\phi(\zeta) \cdot z_\zeta^{\frac{1}{2}} d\zeta + \varsigma \overline{\phi(\zeta)} \cdot (z_{\bar{\zeta}})^{\frac{1}{2}} d\bar{\zeta}. \tag{2.26}$$

Computing their Wirtinger derivatives in the ζ variable and using the almost everywhere relation (2.22), one sees directly that g satisfies a *conjugate* Beltrami equation

$$g_{\overline{\zeta}} = \overline{\nu} \cdot \overline{g_\zeta} \quad \text{with} \quad \nu := -\frac{(\overline{z}_\zeta)^{\frac{1}{2}}}{(z_\zeta)^{\frac{1}{2}}} = -\frac{\vartheta_\zeta}{z_\zeta} \tag{2.27}$$

where the Beltrami coefficient ν is bounded away from 1 (see [5, Equation (2.30)]) this bound depends again on κ). Indeed, one can see from the identity $\vartheta_\zeta = \vartheta_z z_\zeta + \vartheta_{\bar{z}} \overline{z}_\zeta$ that $|\nu| < 2|\vartheta_z| \leq \kappa < 1$.

The focus on the function g is two fold: beyond being solution to the conjugate Beltrami equation (2.27), it is constructed as the primitive of a continuous differential form and thus inherits some additional a priori regularity. Provided one knows that f is locally bounded, one can deduce directly that

- The function g has bounded distortion (see e.g. [2, Equation (2.27)] for the precise definition), smaller than $\frac{1+\kappa}{1-\kappa}$.
- The function g also belongs to $L^{1,2}_{loc}$. Indeed using the formula $g_\zeta = \bar{\varsigma} f(z(\zeta)) z_\zeta + \varsigma \bar{f}(z(\zeta))\vartheta_\zeta$ and recall that $f(z(\zeta))$ is locally bounded. Since the Jacobian of z satisfies $\mathrm{Jac}(z) := |z_\zeta|^2 - |z_{\bar{\zeta}}|^2 \geq (1-\kappa^2)|z_\zeta|^2$, equation (2.22) ensures that $|z_{\bar{\zeta}}| \leq \kappa |z_\zeta|$ in the ζ parametrization, and it is possible to use the area principle. Namely, $\int_\Omega |z_\zeta|^2 d^2\zeta \leq (1-\kappa^2)^{-1} \int_\Omega \mathrm{Jac}(z) d^2 z = (1-\kappa^2)^{-1} \mathrm{Area}(\Omega) < \infty$. This ensures then that g belongs to $L^{1,2}_{loc}$.

Combining the two previous observations, one can apply the Stoïlov factorization stated in [2, Corollary 5.3.3] which allows to write the factorization $g = \underline{g} \circ p$ with $p : \Omega \to \Omega$ a $\beta(\kappa)$-Hölder homeomorphism and $\underline{g}$ an holomorphic function. In particular, g cannot be constant in an open set except if it is constant everywhere in the domain.

3. Proof of the positive magnetization Theorem 1.1

3.1. **Description of the extended domain.** We now prove Theorem 1.1, which allows to deduce directly Theorem 1.2 as mentioned in Section 1, using the technology recalled in [5, Proof of Corollary 1.4] and originally introduced in [19]. The proof of positive magnetization between opposite boundaries in the alternating wired/free/wired/free spin-Ising setup is done first in a special topological rectangle denoted $\mathcal{R}^\delta_{\mathbf{ext}}$, which corresponds to an extension of the approximation of a rectangle of $\mathcal{S}^\delta$. Once the proof in is performed $\mathcal{R}^\delta_{\mathbf{ext}}$, standard monotonicity arguments (e.g. [18, Theorem 7.6]) regarding the change of boundary conditions for the spin-Ising model allow to deduce the same statements for any discretization of a usual rectangle in $\mathcal{S}^\delta$. The main feature of this extended domain $\mathcal{R}^\delta_{\mathbf{ext}}$ is that its boundary contains two macroscopic pieces of the square lattice, which is enough to obtain a contradiction and prove Theorem 1.1. Those two macroscopic regions are called the square grid districts. It is rather easy to construct, in the extended domain, a precompact sequence of s-holomorphic functions F^δ, associated to 4-points Kadanoff-Ceva correlators. The associated functions H^δ converge in their turn to $h = \int \mathrm{Im}[f^2 dz] + |f|^2 d\vartheta$, at least in the bulk of the extended domain. The contradiction will come from the 'sign of the outer derivative' of h (by this we mean whether h tends to grow or decay near one of its boundary arcs). The introduction of the pieces of the square lattice allows to use the technology developed [14] to ensure that discrete Dirichlet boundary conditions of the function H^δ survive when passing to the continuous limit, at least in the square grid districts. This allows to bypass the use of special cuts introduced [5, Section 5] to control the boundary behavior of H^δ. Let us point out that, instead of the partial rewiring procedure between the wired arcs introduced in [14, Equations (6.3) and (6.4)], we present here a more transparent derivation. Still, the rewiring procedure remains useful if one wants to prove convergence (and not only a lower bound) of correlation in the same 4 points setup.

We start by describing in a more precise way the extended domain where we first prove an analogue of Theorem 1.1. Let $(\mathcal{S}^\delta)_{\delta>0}$ be a sequence of s-embeddings satisfying $\mathrm{Lip}(\kappa,\delta)$ and $\mathrm{Exp\text{-}Fat}(\delta)$. In the following lines and the rest of proof, the quantity $o_{\delta\to 0}(1)$ will be positive and goes to 0 as the mesh size of grid goes to 0, is uniform on compacts of the plane, and determines the speed at which the maximal diameter of the connected components of faces with exponentially small radius vanishes, while we also use the notation $\tilde{o}_{\delta\to 0}(1)$, which represents a positive function that goes to 0 as δ goes to 0, and will count for distances in the $\mathcal{S}^\delta$ plane. We aim to find and extend the approximation of a rectangle of a fixed aspect ratio in $\mathcal{S}^\delta$ such that, one has (see Remark 4.5)

- All the tangential quadrilaterals of the boundary of the extended picture have a radius $r_z \geq \exp(-o_{\delta\to 0}(1)\delta^{-1})$.
- The extended picture contains two macroscopic pieces of the square grid lattice whose faces all have a radius $r_z \geq \exp(-o_{\delta\to 0}(1)\delta^{-1})$.

The special boundary of the special topological rectangle $\mathcal{R}_\delta$ approximates up to $\tilde{o}_{\delta\to 0}(1)$ the rectangle $[-\frac{1}{2}, \frac{1}{2}] \times [-3, 3]$ is constructed using two approximations of the segments $\{\pm\frac{1}{2}\} \times [-4; 4]$ that are then connected with approximations of the vertical segments $\{[-\frac{1}{2}; \frac{1}{2}\} \times \{\pm 3\}$, still with fat enough boundary quads.

Proposition 3.1. *Provided δ is small enough, there exist $\mathcal{R}_\delta$ in $\mathcal{S}^\delta$ as above, such that one can construct (see Figure 6) a finite piece of a proper s-embedding denoted $\mathcal{R}_\delta^{\mathbf{ext}}$, approximating up $\tilde{o}_{\delta\to 0}(1)$ the domain $\Omega = [\frac{-1}{2}; \frac{1}{2}] \times [-5; 5] \cup [\frac{1}{2}; 1] \times [-\frac{9}{2}; -\frac{7}{2}] \cup [-1; -\frac{1}{2}] \times [\frac{7}{2}; \frac{9}{2}]$, such that:*

- *All the boundary quads of $\mathcal{R}_\delta^{\mathbf{ext}}$ have a radius $r_z \geq \exp(-o_{\delta\to 0}(1)\delta^{-1})$.*
- *One has $\mathcal{R}_\delta \subseteq \mathcal{R}_\delta^{\mathbf{ext}}$ and the left and right 'vertical' boundaries of $\mathcal{R}_\delta$ belong the boundary of $\mathcal{R}_\delta^{\mathbf{ext}}$.*
- *$\mathcal{R}_\delta^{\mathbf{ext}}$ contains two pieces of a square lattice in the regions $[\frac{1}{2}; 1] \times [-\frac{9}{2}; -\frac{7}{2}]$ and $[-1; -\frac{1}{2}] \times [\frac{7}{2}; \frac{9}{2}]$ whose quads have a radius $r_z \geq \exp(-10000 o_{\delta\to 0}(1)\delta^{-1})$. Those two regions are called the south and the north square grid district.*
- *The vertices of $\mathcal{S}(G^\circ)$ at the bottom horizontal boundary of the south square grid district are horizontally aligned.*
- *$\mathcal{R}_\delta^{\mathbf{ext}}$ satisfies the assumption $\mathrm{Lip}(\kappa, 5\delta)$.*

Proof. See section 4 for an explicit construction. □

3.2. **Contradiction in the special extended domain.** Let $(\Omega_\delta; a^\delta, b^\delta, c^\delta, d^\delta)$ be a discrete simply connected domain of an s-embedding $\mathcal{S}^\delta$, with two *wired* boundary arcs $(b^\delta c^\delta)^\circ$, $(d^\delta a^\delta)^\circ$ and a two *dual-wired* boundary arcs $(c^\delta d^\delta)^\bullet$ and $(a^\delta b^\delta)^\bullet$ (see [14, Section 6] ,[5, Figure 7] or Figure 7). Here $a^\delta, b^\delta, c^\delta, d^\delta$ are corners, separating the extremities of these four arcs and correspond to the places where the discrete function H^δ defined below has jumps (it is constant along each of the four arcs). One can now define the Kadanoff-Ceva four points observable by setting $X^\delta(\cdot) := \mathbb{E}_{\Omega_\delta}[\chi_{(\cdot)}\mu_{(c^\delta d^\delta)^\bullet}\sigma_{(d^\delta a^\delta)^\circ}]$ via (2.5). It is easy to see that

$$\begin{aligned} X^\delta(a^\delta) &= \pm\mathbb{E}_{\Omega_\delta}[\mu_{(a^\delta b^\delta)^\bullet}\mu_{(c^\delta d^\delta)^\bullet}], & X^\delta(d^\delta) &= \pm 1, \\ X^\delta(b^\delta) &= \pm\mathbb{E}_{\Omega_\delta}[\mu_{(a^\delta b^\delta)^\bullet}\mu_{(c^\delta d^\delta)^\bullet}\sigma_{(b^\delta c^\delta)^\circ}\sigma_{(d^\delta a^\delta)^\circ}], & X^\delta(c^\delta) &= \pm\mathbb{E}_{\Omega_\delta}[\sigma_{(b^\delta c^\delta)^\circ}\sigma_{(d^\delta a^\delta)^\circ}]. \end{aligned}$$

Choosing properly the global additive constant in the definition of H_{X^δ} associated to X^δ via (2.17), one has

$$\begin{aligned} H_{X^\delta}((c^\delta d^\delta)^\bullet) &= 1, & H_{X^\delta}((d^\delta a^\delta)^\circ) &= 0, \\ H_{X^\delta}((a^\delta b^\delta)^\bullet) &= 1 - \mathbb{E}[\mu_{(a^\delta b^\delta)^\bullet}\mu_{(c^\delta d^\delta)^\bullet}]^2, & H_{X^\delta}((b^\delta c^\delta)^\circ) &= 1 - \mathbb{E}[\sigma_{(b^\delta c^\delta)^\circ}\sigma_{(d^\delta a^\delta)^\circ}]^2. \end{aligned}$$

We focus on the specific situation where $(\Omega_\delta; a^\delta, b^\delta, c^\delta, d^\delta)$ is the topological rectangle $\mathcal{R}_\delta^{\mathbf{ext}}$ constructed in Section 4 equipped with the Ising model, approximating the domain Ω. Up to passing to another subsequence, one can also assume that $(\mathcal{Q}^\delta)_{\delta>0}$ converges uniformly to a $\kappa < 1$ Lipschitz function ϑ on compacts subsets of the box $[-10; 10]^2$ (recall that the functions $\mathcal{Q}^\delta$ are automatically 1-Lipschitz and defined up to additive constant). One denotes by F^δ and $H^\delta = H_{F^\delta} = H_{X^\delta}$ the functions naturally associated to the correlator X^δ define above via (2.14) and (2.17). Using the maximum principle for H^δ coming from Proposition 2.7, one directly deduces from the boundary conditions (3.2) that the functions H_{F^δ} are uniformly bounded by 1 on Ω_δ. Recall that all the boundary faces of $\mathcal{R}_\delta^{\mathbf{ext}}$ have by construction a radius $r_z \geq \exp(-o_{\delta\to 0}(1)\delta^{-1})$ (replacing if needed the original function $o_{\delta\to 0}(1)$ by $10000 o_{\delta\to 0}(1)$). While the assumption $\text{Lip}(\kappa, 5\delta)$ is fulfilled for the domain $\mathcal{R}_\delta^{\mathbf{ext}}$, it is a priori not the case for the assumption $\text{Exp-Fat}(\delta)$ (as one can see within the proof of Proposition (3.1)). Still, Remark 2.9 using that all boundary quads are fat enough ensures there exist a subsequential limit of the family $(F^\delta)_{\delta>0}$ such that, uniformly on compacts of Ω,

$$F^\delta \to f, \quad H_{F^\delta} \to h = \textstyle\int \mathrm{Im}[(f(z))^2 dz] + |f(z)|^2 d\vartheta.$$

It is clear from the discrete estimate $0 \leq H^\delta \leq 1$ that h takes its values in $[0, 1]$. In general $d\vartheta \neq 0$, and f is not holomorphic. Still, the function f *is* holomorphic inside in the two square grid districts, as ϑ is constant there. This also implies that $h = \int \mathrm{Im}[(f(z))^2 dz]$ in that region is a harmonic function in the two square grid districts. Assuming $\mathbb{E}_{\Omega_\delta}[\sigma_{(b^\delta c^\delta)^\circ}\sigma_{(d^\delta a^\delta)^\circ}] \to 0$ as $\delta \to 0$ along one subsequence, we have $H_{X^\delta}((b^\delta c^\delta)^\circ) = 1 - \mathbb{E}_{\Omega_\delta}[\sigma_{(b^\delta c^\delta)^\circ}\sigma_{(d^\delta a^\delta)^\circ}]^2 \to 1$ as δ goes to 0. The contradiction is obtained in three steps:

- We show that h has Dirichlet boundary values 0 in a piece of the arc of the top left region and has Dirichlet boundary values 1 in a piece of the bottom right region. This requires to show that discrete Dirichlet boundary conditions for the function H^δ survive when passing to the continuous limit.

- The *sign of the outer derivative* of the functions H^δ depends on the type of the arc (i.e. wired or free), at least in the square grid regions. In particular, discrete functions H^δ tend to grow near wired arcs while the continuous functions h has to decay near that same arc by the maximum principle (recall that $h \in [0,1]$ thus h cannot increase near that part of the boundary). At the level of observables, this will translate in the fact that functions F^δ are purely real at the discrete bottom boundary of the southern district while continuous function f is purely imaginary at that boundary. This leaves the only option that f vanishes identically at that arc and thus in the entire southern square grid district.
- The Sloïlov factorization for $I_{\mathbb{C}}[f]$ implies that the function f should actually vanish everywhere in Ω, contradicting the change of boundary values of h between different districts.

The author is grateful to Mikhail Basok for pointing out the Stoïlov factorization allowing to obtain the final contradiction.

Proof. Proof of Theorem 1.1 in $\mathcal{R}_\delta^{\mathbf{ext}}$

Step 1: Boundary behavior of the continuous functions f and h

The proof can be followed with Figure 6. Recall that we assume that the correlation $\mathbb{E}_{\Omega_\delta}[\sigma_{(b^\delta c^\delta)^\circ}\sigma_{(d^\delta a^\delta)^\circ}]^2$ vanishes in the limit along one subsequence as $\delta \to 0$, thus $H_{X^\delta}((b^\delta c^\delta)^\circ) = 1 - \mathbb{E}_{\Omega_\delta}[\sigma_{(b^\delta c^\delta)^\circ}\sigma_{(d^\delta a^\delta)^\circ}]^2 \to 1$ at the wired arc $(b^\delta c^\delta)$. This statement remains in particular true at the horizontal arcs of the bottom right square grid district. *In the square grid districts and a priori only there*, one can apply [14, Proposition 3.6] and deduce directly that

- The function H_{F^δ} is *sub-harmonic* on G° for the natural Laplacian on G° defined in [14, Equation (3.1)].
- The function H_{F^δ} is *super-harmonic* on $G^\bullet$ for the natural Laplacian on $G^\bullet$ defined in [14, Equation (3.1)].

Using the *boundary modification trick* of [14, Lemma 3.14, Remark 3.15] to compare H^δ with discrete harmonic functions proves, exactly as in [14, Theorem 4.3]) that discrete Dirichlet boundary conditions survive when passing to continuum i.e. h extends continuously to 1 at the horizontal arc of the bottom right square grid district. In continuum, the 1 Dirichlet boundary conditions of h at the horizontal segment $[\frac{1}{2};1] \times \{-\frac{9}{2}\}$ (drawn in orange in Figure 6) and the fact that $0 \le h \le 1$ imply that f extends continuously up to the bottom boundary of the square grid district. Moreover, $f^2 \in \mathbb{R}^-$ near that arc, i.e. $f \in i\mathbb{R}$, as in [5, Proof of Theorem 1.3]. One can also note that a similar reasoning on survival of Dirichlet boundary conditions applied at the top square grid district proves that $h = 0$ near the upper vertical segments of its boundary.

Step 2: Boundary behavior of discrete functions F^δ

For discrete observables F^δ, at a boundary quad $z_\partial \in \mathcal{S}^\delta(\diamondsuit(G))$ of the arc approximating the horizontal segment $[\frac{1}{2};1] \times \{-\frac{9}{2}\}$, the increment of H_{F^δ} between two consecutive (from left to right) vertices of $\mathcal{S}(G^\circ)$ vanishes identically (this is a direct consequence of (3.2)). That same increment is also positively proportional to $\mathrm{Im}[F^\delta(z_\partial)^2]$. This allows to conclude that $F^\delta(z_\partial)^2 \in \mathbb{R}$ and one can even go beyond that observation, as the value of the boundary argument of $F^\delta(z_\partial)$ is given directly by the formula [5, Lemma 5.3], which implies that $F^\delta(z_\partial) \in \mathbb{R}$. In particular

$F^\delta(z_\partial)$ is purely real at the boundary, which means that $z' \mapsto \mathrm{Im}[F^\delta(z')]$ vanishes identically at the bottom boundary of the south square grid district.

In the square grid district, $z' \mapsto \mathrm{Im}[F^\delta(z')]$ is a martingale for the standard random walk on quads (i.e. the probability to leave from $z \in \diamondsuit(G)$ to one of its four neighbors is $\frac{1}{4}$). This is a simple implication of the discrete Cauchy-Riemann equation satisfied by F^δ (see e.g. [8, Equation (3.1)]). Set $z_0 = (\frac{3}{4}; -\frac{9}{2} + s)$ and denote by $\mathcal{R}^\delta_{s^{\frac{1}{4}}}$ the square of width $2s^{\frac{1}{4}}$ centered at $(\frac{3}{4}; -\frac{9}{2} + s^{\frac{1}{4}})$. Using the standard gamblers ruin estimates for random walks on $\mathbb{Z}^2$, the probability that the random walk associated to $\mathrm{Im}[F^\delta(z')]$ leaves $\mathcal{R}^\delta_{s^{\frac{1}{4}}}$ from its top side is $O(s^{\frac{3}{4}})$. On the other hand, using uniform crossing estimates for the standard random walk, the probability that this walk leaves $\mathcal{R}^\delta_{s^{\frac{1}{4}}}$ from one of its vertical sides at a vertical distance ρ from the bottom boundary of $\mathcal{R}^\delta_{s^{\frac{1}{4}}}$ is bounded by $\rho^{\frac{1}{2}+\varepsilon}$, for some $\varepsilon > 0$ which is independent from s and $\tilde{\delta}$ (the mesh size of the square lattice in the southern district). We apply now the optional stopping theorem to the time the walk started at z_0 exits $\mathcal{R}^\delta_{s^{\frac{1}{4}}}$ to reconstruct the value $\mathrm{Im}[F^\delta(z_0)]$. One has

- The contribution to $\mathrm{Im}[F^\delta(z_0)]$ coming from the bottom side of $\mathcal{R}^\delta_{s^{\frac{1}{4}}}$ vanishes identically as $\mathrm{Im}[F^\delta]$ vanishes there (which is a consequence of the discussion above).
- The contribution of the top side is bounded by $O(s^{\frac{3}{4}} \cdot s^{-\frac{1}{8}})$ as F^δ is bounded there by $s^{-\frac{1}{8}}$ in the top segments of $\mathcal{R}^\delta_{s^{\frac{1}{4}}}$.
- The contribution of the vertical sides is polynomially small in s, as the probability to leave from one of the vertical sides at a height ρ from the bottom side is bounded by $\rho^{\frac{1}{2}+\varepsilon}$ and we have the bound $|F^\delta(z)| = O(\mathrm{dist}(z, \partial\Omega)^{-\frac{1}{2}})$. To get this bound on the southern district formed by a square grid of mesh size $\tilde{\delta}$, one has to separate two cases.
  - If the distance from z to the bottom boundary is larger than $\mathrm{cst}\tilde{\delta}$ (for some uniform constant cst), one can apply Corollary 2.8.
  - if the distance from z to the bottom boundary is smaller than $\mathrm{cst}\tilde{\delta}$, the reconstruction of F^δ via X^δ given in (2.14) ensures directly that $F^\delta = O(\tilde{\delta}^{-\frac{1}{2}})$.

All together, this ensures that $|\,\mathrm{Im}[F^\delta(z_0)]| = O(s^{\beta''})$ for some positive exponent β''. Sending first δ to 0 and then s to 0 implies that f is purely real at $(\frac{3}{4}; -\frac{9}{2})$ and thus has to vanish at that point, as it is also purely imaginary according the step 1 of the proof given above). Repeating the same reasoning ensures f in fact vanishes in the entire bottom arc of the south square grid district. Since f is holomorphic in the square grid district and vanishes on a boundary arc, it vanishes everywhere in the bottom square grid district. This implies that its primitive $I_\mathbb{C}$ is constant in that region.

Step 3: Final contradiction using the Stoïlov factorization

We are now in position to conclude the final contradiction. Consider the function $g(\zeta) = I_\mathbb{C}(\zeta)$ defined by (2.26) in the ζ conformal parametrization of the surface $(z, \vartheta(z))$. As explained in Section 2.5, g satisfies a conjugate Beltrami equation (2.27) with a Beltrami coefficient which is bounded away from 1 (this bound only depends on κ). Moreover g is constant in the bottom square grid district. Writing

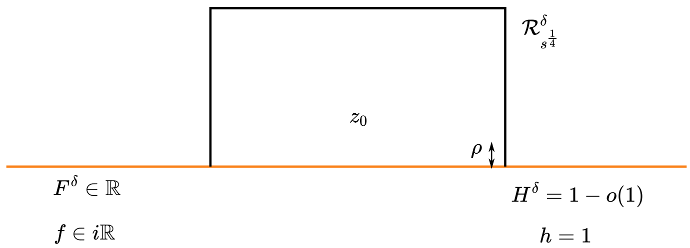

FIGURE 3. Local notation related to the boundary analysis at the south square grid district. The sign of the outer derivative are opposite for discrete H^δ and continuous h, imposing that the continuous observable vanishes at that horizontal arc.

the Stoilov factorization $g = \underline{g} \circ p$ with $p : \Omega \to \Omega$ a $\beta(\kappa)$-Hölder homeomorphism and $\underline{g}$ an holomorphic function, the function $\underline{g}$ is constant in the south square grid district, thus constant everywhere in Ω. In return, this proves that f vanishes everywhere in Ω. This contradicts the change of boundary values from 0 to 1 for the function $h = \int \mathrm{Im}[f^2dz] + |f|^2 d\vartheta$ between the north and the south square grid districts.

$\square$

4. A PROOF OF PROPOSITION 3.1

In this section, we give a complete proof of Proposition 3.1 when starting with a sequence of s-embeddings that satisfy LIP(κ,δ) and EXP-FAT(δ) . The key step into proving Theorem 1.1 is to to it first in the domain $\mathcal{R}^\delta_{\mathbf{ext}}$ and then deduce the same statement for standard rectangles. We start with a subsection containing reminders of rather simple geometrical features of tangential quadrilaterals. Extending a finite piece of an s-embedding and pasting it to a piece of the square lattice, while remaining in the s-embedding setup (i.e. requiring that all faces $\Lambda(G)$ are tangential quadrilaterals) is not obvious at first sight. Still, one notes that in the case of all boundary vertices aligned along a straight line, there exist rather straightforward extension strategies, either by using symmetry arguments or by pasting layers of kites and squares.

4.1. **Features of tangential quadrilaterals.** In the following list of claims, we recall simple geometrical features on tangential quadrilaterals. The claims are illustrated by Figure 4. On s-embeddings that satisfy LIP(κ,δ) for some fixed $\kappa < 1$, all the edges of any quad of $\mathcal{S}^\delta(\diamondsuit(G))$ are of length smaller than δ. Indeed, along the edges of a quad z, the origami map $\mathcal{Q}^\delta$ is real a linear function with rate of growth ± 1. To lighten the notations, we identify each vertex of $\Lambda(G)$ with its image in $\mathcal{S}^\delta(\Lambda(G)$ in the embedding.

Let $z = (v_0^\circ v_0^\bullet v_1^\circ v_1^\bullet)$ be a tangential quadrilateral with an inner circle of radius r_z and centered at $\hat{z}$. In what follows, we do not ask for the convexity of z, but always assume all its edges are of length smaller than δ. Then one has:

(A) The four bisectors of the angles of the quadrilateral z intersect at $\hat{z}$.
(B) The area of the tangential quadrilateral is a product of the radius of its inscribed circle r_z by the half-perimeter of z. In the following paragraphs,

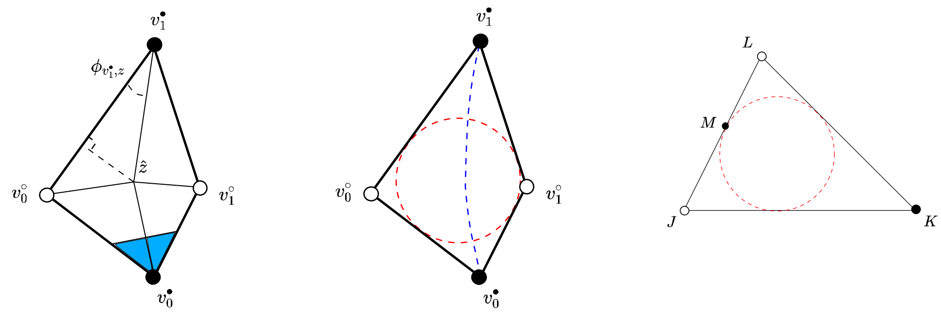

FIGURE 4. (Left) Notations for the tangential quadrilateral with center $\hat{z}$. The four bisectors intersect at the center $\hat{z}$ of the tangential quadrilateral. (Middle) Hyperbola $\mathcal{C}$ drawn in blue denoting in claim (E) the set of points such that $(v_0^\circ v_0^\bullet v_1^\circ v^\bullet)$ is a tangential quadrilateral. (Right) Transformation described in (F) of a triangle into a tangential quadrilateral by adding as a vertex to tangent point of $\mathfrak{C}$ and one of its sides.

in several occasions, we will bound from below the radius of a tangential quad. This is done by bounding from below the area of z and from above its perimeter.

(C) Let $\phi_{v,z}$ be one of the half-angles of z at v (i.e. the angle formed by an edge containing v and the bisector that links v to $\hat{z}$). Then, provided the angle $\phi_{v,z}$ is smaller than $\frac{\pi}{4}$, there exists a universal constant C such that $\phi_{v,z} \geq C \tan \phi_{v,z} \geq C \frac{r_z}{\delta}$. The left inequality is true when $\phi_{v,z}$ goes to 0 while the right inequality is a direct computation on the straight triangle formed by $v, \hat{z}$ and the orthogonal projection of $\hat{z}$ on one of the edges containing v.

(D) Fix an edge $e = [v^\circ v^\bullet]$ of a tangential quadrilateral z attached to vertices v° and $v^\bullet$ whose respective angles are $\phi_{v^\circ,z}$ and $\phi_{v^\bullet,z}$. The length of the edge e equals $r_z(\cot(\phi_{v^\circ,z}) + \cot(\phi_{v^\bullet,z})) \geq r_z \sin(\phi_{v^\circ,z} + \phi_{v^\bullet,z})$.

(E) Fix three vertices $v_{0,1}^\circ$ and $v_0^\bullet$. The set $\mathcal{C}$ of points $v^\bullet$ in the plane such that $(v_0^\circ v_0^\bullet v_1^\circ v^\bullet)$ is a tangential quadrilateral is an *hyperbola* (potentially degenerated to a straight line) passing through $v_0^\bullet$ and $v_1^\bullet$. Indeed, denoting (x, y) the coordinates of $v^\bullet$ and writing the equality $|v^\bullet - v_0^\circ| - |v^\bullet - v_1^\circ| = |v_0^\bullet - v_0^\circ| - |v_0^\bullet - v_1^\circ|$, one recovers the algebraic equation of an hyperbola. The conical $\mathcal{C}$ is clearly unbounded and admits the bisector of the angle $(v_0^\circ v_0^\bullet v_1^\circ)$ as an asymptote when $v^\bullet$ goes to infinity.

(F) Let $T = (JKL)$ be a triangle (whose vertices are labeled in the counter-clockwise order) and consider $\mathfrak{C}$ the circle of radius r which is tangential to its three sides. Consider e.g. M the point at the intersection of $\mathfrak{C}$ and the segment $[JL]$. Then one can view the quadrilateral $(JKLM)$(still labeling vertices in the counter-clockwise order) as a tangential quadrilateral, whose tangential circle is $\mathfrak{C}$.

4.2. **Horizontal alignment of the lattice.** The now present the welding procedure of a piece of a given s-embedding $\mathcal{S}^\delta$ to a piece of the square lattice. The local constrain of all quadrilaterals being tangential is rather unpleasant to handle, thus we will first straighten the boundary by aligning along the same line all its vertices, which provides a simpler situation to handle. The first step is to *slice* horizontally a piece of an s-embedding to extend it afterwards by periodic layers. We present now a very concrete method to replace the intersection of a tangential quadrilateral and a closed half-plane by a similar picture but this time with bottom boundary vertices all aligned along the border of that half-plane. We give the construction for vertical half-planes, but it is rather straightforward to adapt for general half-planes.

Definition 4.1. Let $z \in \diamondsuit(G)$ a tangential quadrilateral, $\overline{z}$ the topological closure of z and y a horizontal level intersecting z away from its vertices. We say that $Z \subseteq \overline{z}$ is a *horizontal alignment* from above of z at level y if

- Z is the union of at most 3 tangential quadrilaterals (see Figure **??**).
- $Z = \overline{z} \cap (iy + \overline{\mathbb{H}})$ i.e. Z is the intersection of z and the close half plane above level y.

One can define in a similar fashion horizontal alignment from below, which concerns the close half plane below level y. The next lemma ensures that it is possible to perform a horizontal alignment (from above or from below) of a given tangential quadrilateral.

Lemma 4.2. *Let z a tangential quadrilateral and y a vertical level (represented by the line iy in $\mathbb{C}$) that intersects z at a level that doesn't contain its highest vertex. Then there exist an horizontal alignment from above of z at level y.*

Proof. The proof is made by an explicit construction using the facts recalled above. We make a dichotomy depending on the number of vertices of z below level y. We encourage the reader to follow the proof with the pictures of Figure **??**.

(1) There is only one vertex of z below level y

Up to swapping colors, one can assume that the vertex below level y is $v_0^\bullet$. Let $\mathcal{C}$ the be hyperbola (claim (E)) of points $v^\bullet$ such that $(v_0^\circ v_1^\bullet v_1^\circ v^\bullet)$ is a tangential quadrilateral. This hyperbola is a continuous curve *inside* z containing the points $v_0^\bullet$ and $v_1^\bullet$. A continuity argument ensures the existence of a point $\tilde{v}^\bullet$ with $\mathrm{Im}[\tilde{v}^\bullet] = y$ such that $(v_0^\circ v_1^\bullet v_1^\circ \tilde{v}^\bullet)$ is a tangential quadrilateral. As a consequence (e.g. checking the alternate sum of edge-lenghts), the quadrilateral $(v_0^\circ v_0^\bullet v_1^\circ \tilde{v}^\bullet)$ is also tangential. Set now the points $\tilde{v}_0^\bullet$ and $\tilde{v}_1^\bullet$ to be respectively the intersections of the segments $[v_0^\circ v_0^\bullet]$ and $[v_0^\circ v_1^\bullet]$ with the level y. Using the claim (F), one can transform the triangles $(\tilde{v}^\bullet v_0^\circ \tilde{v}_0^\bullet)$ and $(\tilde{v}^\bullet v_1^\circ \tilde{v}_1^\bullet)$ as tangential quadrilaterals by adding repectively the vertices $\tilde{v}_{0,y}^\circ$ and $\tilde{v}_{1,y}^\circ$ to the segments $[\tilde{v}_0^\bullet \tilde{v}^\bullet]$ and $[\tilde{v}_1^\bullet \tilde{v}^\bullet]$.

(2) There are two vertices of z below level y

We make a dichotomy of the two subcases that appear here.

(a) The two vertices that lie below level y, $v_0^\bullet$ and v_0°, are of different colors. Consider first $\mathcal{C}_1$ the hyperbola of points $v^\bullet$ such that $(v_0^\circ v_0^\bullet v_1^\circ v^\bullet)$ is a tangential quadrilateral linking continuously $v_0^\bullet$ to $v_1^\bullet$ inside z. There exists once again of a point $\tilde{v}^\bullet$, with $\mathrm{Im}[\tilde{v}^\bullet] = y$, such that $(v_0^\circ v_0^\bullet v_1^\circ \tilde{v}^\bullet)$ is a tangential quadrilateral. As previously, the quadrilateral $(v_0^\circ v_1^\bullet v_1^\circ \tilde{v}^\bullet)$ is tangential. One then reapply the same strategy, this time to the tangential quadrilateral $(v_0^\circ v_1^\bullet v_1^\circ \tilde{v}^\bullet)$ to construct inside $(v_0^\circ v_0^\bullet v_1^\circ \tilde{v}^\bullet)$ a tangential quadrilateral $(v_1^\circ v_1^\bullet \tilde{v}^\circ \tilde{v}^\bullet)$ with $\mathrm{Im}[\tilde{v}^\circ] = y$. Set this time

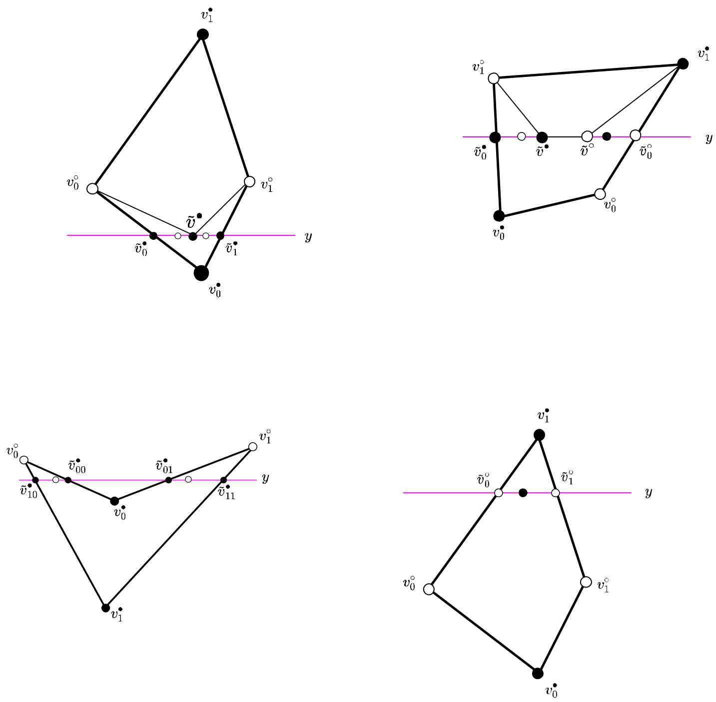

FIGURE 5. Top: (Left) Case 1 (Right) Case 2a. Bottom: (Left) Case 2b (Right) Case 3

$\tilde{v}_0^\bullet$ and $\tilde{v}_0^\circ$ the respective intersections of the segments $[v_1^\circ v_0^\bullet]$ and $[v_1^\bullet v_0^\circ]$ with the line y. Using claim (F), one can construct two tangential quadrilaterals out of the triangles $(\tilde{v}_0^\bullet v_1^\circ v_0^\bullet)$ and $(\tilde{v}_{0,y}^\circ v_1^\bullet v_0^\circ)$ by adding respectively one white vertex to the segment $[\tilde{v}_0^\bullet v^\bullet]$ and one black vertex to the segment $[\tilde{v}_0^\circ \tilde{v}^\circ]$, both located on the axis y.

(b) The two vertices $v_0^\bullet$ and $v_1^\bullet$ below level y are of the same color (that we assume to be black here up to swapping colors). In that case, $(v_0^\circ v_0^\bullet v_1^\circ v^\bullet)$ is non convex and $\overline{z} \cap (iy + \overline{\mathbb{H}})$ is formed by two triangles containing respectively v_0° and v_1°. Denote by $\tilde{v}_{00}^\bullet, \tilde{v}_{01}^\bullet, \tilde{v}_{10}^\bullet, \tilde{v}_{11}^\bullet$ the intersections of respectively $[v_0^\bullet v_0^\circ], [v_0^\bullet v_1^\circ], [v_1^\bullet v_0^\circ], [v_1^\bullet v_1^\circ]$ and this axis y. Then the triangles $(\tilde{v}_{10}^\bullet \tilde{v}_{10}^\bullet v_0^\circ)$ and $(\tilde{v}_{01}^\bullet \tilde{v}_{11}^\bullet v_1^\circ)$ can be viewed as tangential quadrilaterals by adding two white vertices to the segments $[\tilde{v}_{10}^\bullet \tilde{v}_{00}^\bullet]$ and $[\tilde{v}_{01}^\bullet \tilde{v}_{11}^\bullet]$ using claim (F).

(3) There are three vertices of z below level y

Assume e.g. that $v_1^\bullet$ lies above level y. The consider $\tilde{v}_0^\circ$ and $\tilde{v}_1^\circ$ the intersections of y and the segments $[v_1^\bullet v_0^\circ]$ and $[v_1^\bullet v_1^\circ]$. Then one can view the triangle $(v_1^\bullet \tilde{v}_0^\circ \tilde{v}_1^\circ)$ as a tangential quadrilateral by adding a black vertex to the segment $[\tilde{v}_0^\circ \tilde{v}_1^\circ]$, using again claim (F).

□

In our proof, in order to apply regularity theory for s-holomorphic function, it is enough to check that the extended picture constructed has a boundary formed of tangential quadrilaterals that all have a radius larger than $r_z \geq \exp(-o_{\delta\to 0}(1)\delta^{-1})$. In principle, if we are not careful when choosing the slicing level and use some symmetry techniques to extend the picture, it might happen that the newly constructed boundary is composed of quads with exponentially small radii, not allowing to use of regularity theory for s-holomorphic functions developed in Section 2.4. We explain now that, if one starts with a quad in $\mathcal{S}^\delta$ whose radius not so small, there is only a small share of vertical levels intersecting that will produce horizontal alignments with too small of a radii. The next definition precises this idea.

Definition 4.3. Let y be a horizontal a level that intersects the tangential quad z. We say that y is a *β-bad level* for z if one of the tangential quadrilaterals constructed with the algorithm of the horizontal alignment from above of Lemma 4.2 has a radius r_z smaller than β. The complement of β-bad levels are called *β-good levels*.

The next proposition upper bounds the share of bad levels in a tangential quadrilateral z whose radius is larger than $\exp(-\gamma\delta^{-1})$. Informally speaking, the proof shows that $\beta-$bad levels (for a small β) are only those close to the horizontal lines containing vertices of z.

Proposition 4.4. *Let z be a tangential quad with a radius $r_z \geq \exp(-\gamma\delta^{-1})$ and whose edges are all of length smaller than δ. Then provided δ is small enough, the (vertical) one dimensional Lebesgue measure of $\exp(-40\gamma\delta^{-1})$-bad levels intersecting z is at most $4\exp(-4\gamma\delta^{-1})$.*

Proof. We work with δ chosen small enough. Using claim (C) on the features of tangential quadrilateral, the angles $\phi_{v,z}$ are bounded from below by $\delta^{-1}\exp(-\gamma\delta^{-1}) \geq \exp(-\gamma\delta^{-1})$, as $r_z \geq \exp(-\gamma\delta^{-1})$ and while edge-lengths of the boundary segments of z are smaller than δ. Fix an horizontal level y, at a vertical distance at least $\exp(-4\gamma\delta^{-1})$ from the (at most) 4 axes containing the vertices of z and perform an horizontal alignment at level y following Lemma 4.2. We keep exactly the notations of that Lemma and treat separately the four subcases presented there, depending on the number of vertices below level y. We still denote $\hat{z}$ the center of the tangential quadrilateral.

(1) There is only one vertex of z below the axis y

One claims that, provided δ is small enough, the area of the tangential quadrilaterals $(v_0^\circ v_1^\bullet v_1^\circ \tilde{v}^\bullet)$ and $(v_0^\circ v_0^\bullet v_1^\circ \tilde{v}^\bullet)$ can be bounded from below by the quantity $\frac{1}{2}\exp(-\gamma\delta^{-1})\exp(-4\gamma\delta^{-1})\exp(-4\gamma\delta^{-1}) \geq \exp(-10\gamma\delta^{-1})$. To do that, we are first lower bound the area the of tangential quadrilateral $(v_0^\circ v_0^\bullet v_1^\circ \tilde{v}^\bullet)$, then lower bound one of its angles and derive the statement for $(v_0^\circ v_1^\bullet v_1^\circ \tilde{v}^\bullet)$ and $(v_0^\circ v_0^\bullet v_1^\circ \tilde{v}^\bullet)$.

Consider e.g. the triangle (filled in blue in the left Figure 4) denoted by $T_{(v_0^\circ v_0^\bullet v_1^\circ \tilde{v}^\bullet)}(v_0^\bullet, \exp(-4\gamma\delta^{-1})) = T(v_0^\bullet, \exp(-4\gamma\delta^{-1})) \subseteq (v_0^\circ v_0^\bullet v_1^\circ \tilde{v}^\bullet)$, isoscele at $v_0^\bullet$ such that

- The symmetry axis of $T(v_0^\bullet, \exp(-4\gamma\delta^{-1}))$ is the bisector of the angle $(v_0^\circ v_0^\bullet v_1^\circ)$
- Two sides of $T(v_0^\bullet, \exp(-4\gamma\delta^{-1}))$ belong respectively to the segments $[v_0^\circ v_0^\bullet]$ and $[v_1^\circ v_0^\bullet]$.

- The height of $T(v_0^\bullet, \exp(-4\gamma\delta^{-1}))$ (along the bisector of the angle $(v_0^\circ v_0^\bullet v_1^\circ)$) is $\exp(-4\gamma\delta^{-1})$.

Since the angle $\widehat{\phi_{v_0^\bullet,z}}$ is bounded from below by $\exp(-\gamma\delta^{-1})$, the area $A_{(v_0^\circ v_0^\bullet v_1^\circ \tilde{v}^\bullet)}$ of $T(v_0^\bullet, \exp(-4\gamma\delta^{-1}))$ and thus the area of $(v_0^\circ v_0^\bullet v_1^\circ \tilde{v}^\bullet)$ is larger than $\exp(-10\gamma\delta^{-1})$. Moreover, the perimeter $\mathrm{Per}_{(v_0^\circ v_0^\bullet v_1^\circ \tilde{v}^\bullet)}$ of $(v_0^\circ v_0^\bullet v_1^\circ \tilde{v}^\bullet)$ is at most 4δ (it is a general fact that if a convex polygon lies inside another one, the perimeter of the outer one is larger than the interior one).

(1) $r_{(v_0^\circ v_0^\bullet v_1^\circ \tilde{v}^\bullet)} = 2A_{(v_0^\circ v_0^\bullet v_1^\circ \tilde{v}^\bullet)}\mathrm{Per}^{-1}_{(v_0^\circ v_0^\bullet v_1^\circ \tilde{v}^\bullet)} \geq \frac{1}{2}\exp(-10\gamma\delta^{-1})\cdot\delta^{-1} \geq \exp(-10\gamma\delta^{-1})$ using claim (B) when δ is small enough.
(2) The angles $\widehat{v_0^\bullet v_0^\circ \tilde{v}^\bullet}$ and $\widehat{v_0^\bullet v_1^\circ \tilde{v}^\bullet}$ are both bounded from below by the quantity $Cr_{(v_0^\circ v_0^\bullet v_1^\circ \tilde{v}^\bullet)}\delta^{-1} \geq C\exp(-10\gamma\delta^{-1})\cdot\delta^{-1} \geq \exp(-10\gamma\delta^{-1})$, where the absolute constant C comes from claim (C) and δ is chosen small enough.
(3) One can compute directly the area of the triangle $[v_0^\bullet v_0^\circ \tilde{v}^\bullet]$, which is exactly equal to $\frac{1}{2}\sin\widehat{v_0^\bullet v_0^\circ \tilde{v}^\bullet}\ |\tilde{v}_0^\bullet - v_0^\circ||\tilde{v}^\bullet - v_0^\circ| \geq \frac{1}{4}\exp(-10\gamma\delta^{-1})\cdot\exp(-4\gamma\delta^{-1})\cdot\exp(-4\gamma\delta^{-1}) \geq \exp(-20\gamma\delta^{-1})$ (as $\sin\widehat{v_0^\bullet v_0^\circ \tilde{v}^\bullet} \geq \frac{1}{2}\exp(-10\gamma\delta^{-1})$ and both distances $|\tilde{v}_0^\bullet - v_0^\circ|$ and $|\tilde{v}_0^\bullet - v_0^\circ||\tilde{v}^\bullet - v_0^\circ|$ are larger than $\exp(-4\gamma\delta^{-1})$). Since the perimeter of $[v_0^\bullet v_0^\circ \tilde{v}^\bullet]$ is smaller than 10δ, one gets the lower bound $r_{v_0^\bullet v_0^\circ \tilde{v}^\bullet \tilde{v}_{0,y}^\circ} \geq \exp(-20\gamma\delta^{-1})$, repeating exactly the area/perimeter argument given in step 1.

The same result holds for the triangle $(v_0^\bullet v_1^\circ \tilde{v}^\bullet)$ viewed as a tangential quadrilateral.

(2) There are two vertices of opposite color of z below the axis y

Recall that the horizontal alignment is constructed by modifying along the appropriate hyperbola $(v_0^\bullet v_1^\circ v_1^\bullet v_0^\circ)$ into $(\tilde{v}^\bullet v_1^\circ v_1^\bullet v_0^\circ)$ and then modifying along the appropriate hyperbola $(\tilde{v}^\bullet v_1^\circ v_1^\bullet v_0^\circ)$ into $(\tilde{v}^\bullet v_1^\circ v_1^\bullet \tilde{v}^\circ)$.

Repeating the arguments of the case with one vertex below the axis y, one gets

- The angles $\widehat{v_0^\bullet v_1^\circ \tilde{v}^\bullet}$ and $\widehat{\tilde{v}^\circ v_1^\bullet v_0^\circ}$ are larger than $\exp(-10\gamma\delta^{-1})$, as in (2). The radii of the tangential quadrilaterals associated to the triangles $(\tilde{v}_0^\bullet v_1^\circ \tilde{v}^\bullet)$ and $(\tilde{v}_0^\circ v_1^\bullet \tilde{v}^\circ)$ are then larger than $\exp(-20\gamma\delta^{-1})$ as (3).
- The tangential quadrilateral $(v_0^\circ \tilde{v}^\bullet v_1^\circ v_1^\bullet)$ has an area at least $\exp(-10\gamma\delta^{-1})$ which implies that both the angle $\widehat{\tilde{v}^\bullet v_1^\circ v_1^\bullet}$ and the radius $r_{v_0^\circ \tilde{v}^\bullet v_1^\circ v_1^\bullet}$ are larger than $\exp(-10\gamma\delta^{-1})$.
- One can now consider the triangle $T_{(v_0^\circ \tilde{v}^\bullet v_1^\circ v_1^\bullet)}(v_1^\circ, \exp(-12\gamma\delta^{-1})) = T(v_1^\circ, \exp(-12\gamma\delta^{-1}))$, isoscele at v_1° whose height along the bisector of $(v_0^\circ \tilde{v}^\bullet v_1^\circ v_1^\bullet)$ is $\exp(-12\gamma\delta^{-1})$. This triangle is contained in $(v_0^\circ \tilde{v}^\bullet v_1^\circ v_1^\bullet)$ and has an area area is $\frac{1}{2}\sin\widehat{\tilde{v}^\bullet v_1^\circ v_1^\bullet}\cdot\exp(-12\gamma\delta^{-1})\cdot\exp(-12\gamma\delta^{-1}) \geq \exp(-40\gamma\delta^{-1})$. One can then conclude that $r_{v_1^\circ \tilde{v}^\bullet \tilde{v}_1^\circ v_1^\bullet} \geq \exp(-40\gamma\delta^{-1})$ as in (1).

(3) Remaining cases To handle the remaining cases (corresponding to 2b and 3 in Lemma 4.2) it is sufficient to note that in e.g. the case where three vertices of z are below the axis y, the triangle $T_{(v_0^\bullet v_0^\circ v_1^\bullet v_1^\circ)}(v_1^\bullet, \exp(-4\gamma\delta^{-1})) = T(v_1^\bullet, \exp(-4\gamma\delta^{-1}))$ is *inside* the triangle $(\tilde{v}_0^\circ v_1^\bullet \tilde{v}_0^\circ)$ has an area at least $\exp(-10\gamma\delta^{-1})$ as the angle of z at $v_0^\bullet$ is bounded from below by $\exp(-\gamma\delta^{-1})$. In particular the tangential quadrilateral associated to the triangle $(\tilde{v}_0^\circ v_1^\bullet \tilde{v}_0^\circ)$ has then a radius $r_z \geq \exp(-10\gamma\delta^{-1})$ as in (3).

All together, this proves that the one dimensional Lebesgue measure (in the vertical direction) of $\exp(-40\gamma\delta^{-1})$-bad levels intersecting z is at most $4\exp(-4\gamma\delta^{-1})$.

□

Remark 4.5. In this remark, we translate the assumption Exp-Fat(δ) in words and explain its consequences. The main features of the assumption Exp-Fat(δ) are the following:

- Fix a straight segment ℓ in an open bounded region U, and parametrize it naturally by $[0;1]$. Then, there exist a positive function $o_{\delta\to 0}(1)$ (which depends on U and not on ℓ), such that, for each $\delta > 0$,
  - There exist an injective sequence of neighboring vertices $(v_i)_{1\leq i\leq I}$ of $\Lambda(G)$ (i.e. such that $v_i \sim v_{i+1}$ in $\Lambda(G)$) such that each v_i belongs only to tangential quadrilaterals whose radius is larger than $\exp(-o_{\delta\to 0}(1)\delta^{-1})$. The edges attached to this sequence of vertices can be naturally viewed as an arc ℓ^δ, parametrized by $[0;1]$.
  - $\sup_{t\in[0;1]}(\ell(t), \ell^\delta(t)) \to 0$ as δ goes to 0. In that case we say that ℓ^δ approximates ℓ.

  In particular, this induces a sequence (z_δ^ℓ) of neighboring tangential quadrilaterals, attached to edges linking consecutive vertices $(v_i)_{1\leq i\leq I}$, staying e.g. always on the left of the arc ℓ^δ, such that all quads (z_δ^ℓ) have a radius larger than $\exp(-o_{\delta\to 0}(1)\delta^{-1})$.
- Fix $\ell_{1,2}$ two different straight segments in U which are parallel to each other and $z_\delta^{\ell_{1,2}}$ two approximating sequences by tangential quads as described above, and ℓ' a segment of U which perpendicular to $\ell_{1,2}$ and intersects both segments. We assume that the intersections of ℓ' doesn't happen neither at the extremities of $\ell_{1,2}$ nor ℓ. Then there exist a sequence of neighboring tangential quadrilaterals (which again can be taken with an injective sequence of boundary vertices) such that all radii in that sequence ar larger than $\exp(-o_{\delta\to 0}(1)\delta^{-1})$ and that connects $z_\delta^{\ell_1}$ and $z_\delta^{\ell_1}$, approximating the segment of ℓ' that is between ℓ_1 and ℓ_2.

To see the first property, assume for simplicity that ℓ is a vertical segment of length 1 and fix $\varepsilon > 0$. Consider the rectangle $A_{\ell,\varepsilon}$ of width 2ε, whose symmetry axis is ℓ. When covering $A_{\ell,\varepsilon}$ with $\mathcal{S}^\delta$ and removing the connected components of the vertices in $\mathcal{S}^\delta \cap A_{\ell,\varepsilon}$ belonging to tangential quadrilaterals whose associated radii are smaller than $\exp(-o_{\delta\to 0}(1)\delta^{-1})$, there exist a sequence of neighboring vertices in $A_{\ell,\varepsilon} \cap \mathcal{S}^\delta$, all belonging only to tangential quadrilaterals whose radius is larger than $\exp(-o_{\delta\to 0}(1)\delta^{-1})$, which connects $\tilde{o}_{\delta\to 0}(1)$ close to the top of $A_{\ell,\varepsilon}$ to $\tilde{o}_{\delta\to 0}(1)$ close to the bottom of $A_{\ell,\varepsilon}$ and not backtracking macroscopically. Either way, this would imply the existence of a macroscopic blocking surface between the top and the bottom, formed by quads with a too small inner radius. This is enough to conclude for the first claim. The second claim is straightforward once the first is obtained, using simple topological arguments.

4.3. **Pasting of a piece of the square lattice.** We are now in prove Proposition 3.1

Proof of Proposition 3.1. We encourage the reader to follow the construction given below using Figure 6. We only treat with greater details the construction and extension the bottom boundary.

Step 1: Determination of central part of the vertical boundaries of $\mathcal{R}_\delta^{\mathbf{ext}}$

Following Remark 4.5, one can find two sequence of neighboring tangential quadrilaterals with large enough inner circle, respectively denoted $\mathcal{W}_\delta$ and $\mathcal{E}_\delta$ that approximate the vertical segments $\{\mp\frac{1}{2}\} \times [-4;4]$ up to $\tilde{o}_{\delta\to 0}(1)$. We focus on the construction of left arc $\mathcal{W}_\delta$, the construction of $\mathcal{E}_\delta$ is similar. First consider a sequence of neighboring vertices (v_i) of $\Lambda(G)$ with alternating colors (i.e. $v_i^\circ \sim v_i^\bullet \sim v_{i+2}^\circ$), that approximates up to $\tilde{o}_{\delta\to 0}(1)$ the segment $\{-\frac{1}{2}\} \times [-4;4]$, attached only to tangential quadrilaterals whose radius satisfies $r_z \geq \exp(-o_{\delta\to 0}(1)\delta^{-1})$. For each triple of consecutive vertices $v_i^\circ \sim v_{i+1}^\bullet \sim v_{i+2}^\circ$ (or $v_i^\bullet \sim v_{i+1}^\circ \sim v_{i+2}^\bullet$) of this injective path ℓ^δ of vertices, one can order, in the counterclockwise direction, all tangential quadrilaterals attached to $v_{i+1}^\bullet$ that lie between the oriented edges $\overrightarrow{v_{i+1}^\bullet v_i^\circ}$ and $\overrightarrow{v_{i+1}^\bullet v_{i+2}^\circ}$. Concatenating this sequences of tangential quadrilaterals in the natural order, this creates the arcs $\mathcal{W}_\delta$ of tangential quadrilaterals such that two neighbors share an edge and all quads are attached to ℓ^δ. At the end of this first step, on gets the two arcs, labeled (starting from the bottom part of the graph) respectively $\mathcal{W}_\delta = (z_k^{w_\delta})_{1\leq k\leq |\mathcal{W}_\delta|}$ and $\mathcal{E}_\delta = (z_k^{e_\delta})_{1\leq k\leq |\mathcal{E}_\delta|}$. The sequences of quads are injective and we have $z_k^{w_\delta} \sim z_{k+1}^{w_\delta}$ and $z_k^{e_\delta} \sim z_{k+1}^{e_\delta}$ in $\diamondsuit(G)$. Both $\mathcal{W}_\delta$ and $\mathcal{E}_\delta$ are represented in purple in Figure 6.

Step 2: Determination of the blue alignment (from above) level

The rest of the construction will be combination of symmetry arguments, horizontal alignments and explicit extensions. Our first goal is to find a vertical level to apply an horizontal alignment from above to *all* tangential quadrilaterals that lie between $\mathcal{W}_\delta$ and $\mathcal{E}_\delta$ intersecting that level, while forcing that leftmost and rightmost created tangential quadrilateral (which are respectively obtained from alignment of quads of $\mathcal{W}_\delta$ and $\mathcal{E}_\delta$) to have a large enough inner circle radius. We explain now the construction in greater details.

There are at most $O(\exp(2o_{\delta\to 0}(1)\delta^{-1}))$ tangential quadrilaterals in $[-10\times 10]^2$ with a radius $r_z \geq \exp(-o_{\delta\to 0}(1)\delta^{-1})$. In particular, there exist a horizontal level $y_b^\delta = \frac{-7}{2} + \tilde{o}_{\delta\to 0}(1)$ (drawn in blue in Figure 6) which remains at a vertical distance at least $10\exp(-4o_{\delta\to 0}(1)\delta^{-1})$ from all vertices of $\Lambda(G)\cap[-10\times 10]^2$ belonging to one of the tangential quadrilaterals with a radius $r_z \geq \exp(-o_{\delta\to 0}(1)\delta^{-1})$. Up to an arbitrary small vertical shift, we can also assume that y_b^δ doesn't intersect any vertex of $\Lambda(G)$ in the box $[-10\times 10]^2$.

Let $1 \leq k_{\mathcal{W}_\delta} \leq |\mathcal{W}_\delta|$ be the index such that the tangential quadrilateral $z_{k_{\mathcal{W}_\delta}}$ intersects the vertical level y_b^δ and such that for any $l > k_{\mathcal{W}_\delta}$, all quads of $\mathcal{W}_\delta$ lie *strictly above* the level y_b^δ. In particular, $z_{k_{\mathcal{W}_\delta}}^{w_\delta}$ is the last quadrilateral of $\mathcal{W}_\delta$ that intersects y_b^δ (meaning that for all $l > k_{\mathcal{W}_\delta}$, the quad $z_l^{w_\delta}$ lies strictly above y_b^δ). Define in a similar way the integer $k_{\mathcal{E}_\delta}$ such that $z_{k_{\mathcal{E}_\delta}}^{e_\delta}$ is the last quadrilateral of $\mathcal{E}_\delta$ that intersects y_b^δ. One then performs a horizontal alignment at level y_b^δ to all tangential quadrilaterals that lie (horizontally) between $z_{k_{\mathcal{W}_\delta}}^{w_\delta}$ and $z_{k_{\mathcal{E}_\delta}}^{e_\delta}$. Due to Proposition 4.4, after this horizontal alignment $z_{k_{\mathcal{W}_\delta}}^{w_\delta}$ and $z_{k_{\mathcal{E}_\delta}}^{e_\delta}$ are each transformed in at most 3 tangential quadrilaterals with a radius $r_z \geq \exp(-40o_{\delta\to 0}(1)\delta^{-1})$.

Step 3 : Determination of the (dashed) red symmetrization level

Recall that the leftmost and the rightmost tangential quadrilaterals attached to the level y_b^δ and between $\mathcal{E}_\delta$ and $\mathcal{W}_\delta$ have both a radius $r_z \geq \exp(-40o_{\delta\to 0}(1)\delta^{-1})$. The level $y_r^\delta = y_b^\delta + 10\exp(-4\times 40o_{\delta\to 0}(1)\delta^{-1}) = y_b^\delta + 10\exp(-160o_{\delta\to 0}(1)\delta^{-1})$

(again slightly shifting vertically if needed) is used to perform an horizontal alignment *from above* at the level y_r^δ to all quadrilaterals intersecting y_r^δ (drawn in red dashes in Figure 6). One obtains thanks to this procedure a 'strip' of height $\tilde{\delta} = 10\exp(-160 o_{\delta\to 0}(1)\delta^{-1})$ and of width $1+\tilde{o}_{\delta\to 0}(1)$, formed by tangential quadrilaterals. Using again Proposition 4.4, the leftmost and the rightmost tangential quadrilaterals of this 'strip' have a radius $r_z \geq \exp(-1600 o_{\delta\to 0}(1)\delta^{-1})$. Denote S_b^r this strip of width $\tilde{\delta}$ and S_r^b the symmetric picture with respect to y_b^δ. Given that $\tilde{\delta} << \exp(-40 o_{\delta\to 0}(1)\delta^{-1})$, it is easy to check that there is indeed only one leftmost and one rightmost tangential quadrilaterals in the strip (meaning that there those extremal quads indeed connect the top to the bottom of the strip), as the alignment from above at level y_b^δ will corresponds this time to the case 3 of the construction of Lemma 4.2.

Step 4 : Perform the symmetrization

We are now going to extend the picture obtained *at the end of step 2* below the blue level y_b^δ by symmetrizing the strip between y_b^δ and y_r^δ. In order to do that, paste (below y_b^δ) alternatively the strips S_r^b and S_b^r until we reach the level $-\frac{9}{2} + \tilde{o}_{\delta\to 0}(1)$, starting with a strip of the type S_r^b and finishing with a strip of the type S_b^r. Finally, we paste to this lowest line the picture symmetric of the region delimited by y_δ^b, the 'vertical' boundaries of $\mathcal{W}_\delta$ and $\mathcal{E}_\delta$ (drawn in purple dashes) and one arc, constructed in a similar fashions as $\mathcal{W}_\delta$ and $\mathcal{E}_\delta$ that connects the last two mentioned arcs using tangential quads all with a radius $r_z \geq \exp(-o_{\delta\to 0}(1)\delta^{-1})$ while approximating the level $y = -3 + \tilde{o}_{\delta\to 0}(1)$ (the arc is drawn in green solid line while its symmetric is drawn in green dashes). Here the fact that all tangential quadrilaterals of the arcs $\mathcal{W}_\delta$ and $\mathcal{E}_\delta$ whose respective labels are larger than $k_{\mathcal{W}_\delta}$ and $k_{\mathcal{E}_\delta}$ are above y_b^δ ensure that the obtained picture is proper as there is no overlap with the symmetrization.

Step 5: Pasting kites then squares

The strip region is a sequence of alternating strips S_r^b and S_b^r, pasted below each other. In particular, since the construction is made using symmetries, the vertex right boundary of the strip region (in green solid in Figure 6) is delimited by a sequence of neighboring vertices of $\Lambda(G)$, labeled (up to swapping colors by) $v_{2k}^\bullet \in G^\bullet$, $v_{2k+1}^\circ \in G^\circ$, and $v_i \sim v_{i+1}$ in $\Lambda(G)$. In our case, we label vertices in the natural order, from top to bottom. One can see that $\mathrm{Re}[v_{2k}^\bullet] = \mathrm{Re}[v_{2k+2}^\bullet]$, $\mathrm{Re}[v_{2k+1}^\circ] = \mathrm{Re}[v_{2k+3}^\circ]$ and $\mathrm{Im}[v_i] - \mathrm{Im}[v_{i+2}] = 2\tilde{\delta}$. Let $x^\delta = \max(\mathrm{Re}[v_2^\bullet], \mathrm{Re}[v_3^\circ])$, which represents the rightmost point of the slit region. We treat the case where this rightmost point belongs to $G^\bullet$, a similar treatment can be easily done if it belongs to G°. One can construct a vertical layer of *kites* formed by the points $v_{2k}^\bullet, v_{2k+1}^\circ, v_{2k}^\bullet$ and $\tilde{v}_{2k+1}^\circ = v_{2k}^\bullet - i\tilde{\delta} + \tilde{\delta}$. This kite has an area larger than the straight triangle $(v_{2k}^\bullet v_{2k+2}^\bullet \tilde{v}_{2k+1}^\circ)$ whose area is $\frac{1}{2}\tilde{\delta}^2$. In particular it is not hard to see that radius of the inner circle of one of those kites is at least $\tilde{\delta}^4$. Once this first layer of kites is constructed for the right part strip region, the right part of the vertex boundary of the strip region is now formed by a sequence of neighboring vertices in $\Lambda(G)$, with vertices of $G^\bullet$ vertically aligned, vertices of G° vertically aligned, and boundary edges (seen as vectors oriented from $G^\bullet$ to G°) taking alternatively the values $\sqrt{2}\tilde{\delta}e^{\pm i\frac{\pi}{4}}$. It is straightforward to extend this boundary into a region of the square lattice of edge length $\sqrt{2}\tilde{\delta}$. We repeat the same construction in the upper left part of the embedding. We now set the boundary of $\mathcal{R}_{\mathbf{ext}}^\delta$ to be the approximation natural approximation of the domain $\Omega = \big([\frac{-1}{2};\frac{1}{2}]\times[-5;5]\big)\cup\big([\frac{1}{2};1]\times[-\frac{9}{2};-\frac{7}{2}]\cup\big([-1;-\frac{1}{2}]\times[\frac{7}{2};\frac{9}{2}]\big)$, using the boundaries of all pieces constructed in all the steps of the construction, chosen so that all boundary quadrilaterals of $\mathcal{R}^{\delta}_{\mathbf{ext}}$ have a radius $r_z \geq \exp(-10000 o_{\delta\to 0}(1)\delta^{-1})$ and imposing that all vertices of G° belonging to the lower horizontal arc of the south left district are horizontally aligned.

Step 6: Checking the Lip condition

One still needs to check that the constructed picture $\mathcal{R}^{\delta}_{\mathbf{ext}}$ satisfies $\mathrm{Lip}(\kappa, 5\delta)$. When computing the increment of the origami map between two points of original part of the graph (before extension), it automatically holds, as well as in the square grid regions (where the origami map only takes, up to a global additive constant, the values $\sqrt{2}\tilde{\delta}$ or 0). In the slit regions, the origami map has vertical increment (between two points vertically aligned) at most $2\tilde{\delta} << \delta$ while its horizontal increments corresponds are exactly the same as along y^{δ}_{b}, which also satisfies $\mathrm{Lip}(\kappa, 4\delta)$. Finally, when considering the increment of the origami map between points belonging to two different regions (original embedding, strip regions or square grid districts), it is enough to use the above observations together with the fact that the origami map is trivially 1-Lipschitz for the tiny layers (of size much smaller than δ) of transition between different regions, and thus the above results allow to conclude.

□

We now precise the topological quadrilateral $(\Omega_\delta; a^\delta, b^\delta, c^\delta, d^\delta)$ seen as a discrete simply domain in $\mathcal{S}^\delta$ with two wired boundary arcs $(b^\delta c^\delta)^\circ$, $(d^\delta a^\delta)^\circ$ and a two dual-wired boundary arcs $(c^\delta d^\delta)^\bullet$ and $(a^\delta b^\delta)^\bullet$ (see [14, Section 6], [5, Figure 7] or Figure 7) using $\mathcal{R}^{\mathbf{ext}}_{\delta}$. We started with an injective path ℓ^δ in $\Lambda(G)$ approximating a segment and such that all the vertices of that path only belong to quads with a large enough radius. Labeling the vertices of ℓ^δ by $(v_k)_{0\leq k\leq 2n}$ assuming e.g. that $v_{2i} = v^\circ_{2i} \in G^\circ$ and $v_{2i+1} = v^\bullet_{2i+1} \in G^\bullet$, one gets for each $v^\bullet_{2i+1}$ of ℓ^δ, to a sequence of counterclockwise ordered tangential quads between the vectors $\overrightarrow{v^\bullet_{2i+1}v^\circ_{2i}}$ and $\overrightarrow{v^\bullet_{2i+1}v^\circ_{2i+2}}$ (and similarly for v°_{2i}). Concatenating them in the natural order along the boundary of $\mathcal{R}^{\mathbf{ext}}_{\delta}$, one then gets a sequence of neighboring tangential quadrilaterals (z_k) attached to the vertex boundary of $\mathcal{R}^{\mathbf{ext}}_{\delta}$. One can now apply a construction of the alternating Dobrushin arcs, similar to [14, Figure 2] or [5, Figure 7]. Each wired arc can be viewed as a sequence of *boundary half quads* $(v^\circ_{2i}v^\bullet_{2i+1}v^\circ_{2i+2}z_i)$ (see [5, Section 5.3]) with $z_i \in \diamondsuit(G)$ and all three vertices $v^\circ_{2i}, v^\bullet_{2i+1}, v^\circ_{2i+2}$ belonging to z_i. From a statistical mechanics perspectives, all the faces attached to that arc are wired, and all attached spins are in fact a single one. Similarly all disorders attached to a free arc are in fact a single disorder. The corners $a^\delta, b^\delta, c^\delta, d^\delta$ correspond to edges of $\Lambda(G)$ linking the four arcs. In the case we use here, the boundary of $(\Omega_\delta; a^\delta, b^\delta, c^\delta, d^\delta)$ is constructed using the one of $\mathcal{R}^{\mathbf{ext}}_{\delta}$ and is formed by:

- Two free arcs approximating respectively the segments $\{\mp\frac{1}{2}\}\times[-3;3]$ seen as a sequence of boundary half-quads originating from the 'vertical' boundary of $\mathcal{R}^{\delta}_{\mathbf{ext}}$.
- A wired arc containing the approximations of $\{-\frac{1}{2}\}\times[-5;3]\cup\{[-\frac{1}{2};\frac{1}{2}]\}\times\{-5\}\cup\{\frac{1}{2}\}\times[-5;-\frac{9}{2}]\cup\{\frac{1}{2}\}\times[-\frac{7}{2};-3]$ together with the bottom (chosen with all boundary quads exactly horizontally aligned), right and upper part of the square grid district.

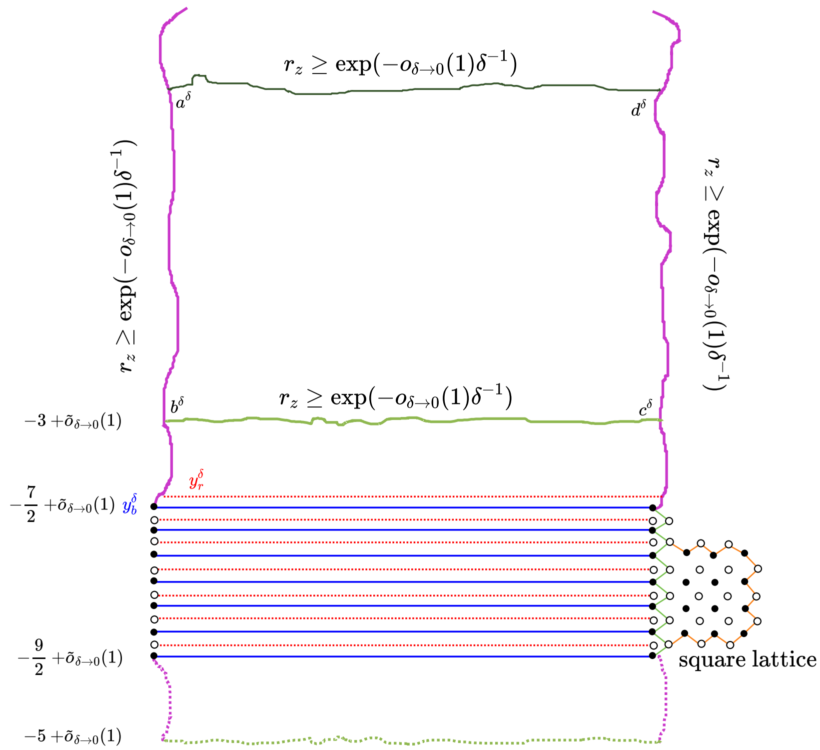

FIGURE 6. Picture attached to the construction of the extended domain $\mathcal{R}^\delta_{ext}$. The slicing line y^δ_b to perform the horizontal alignment from above is drawn in blue solid, while the symmetrization is made using successive copies of the strip between y^δ_r (in red dashes) and y^δ_b. Finally, one pastes a layer of kites and a piece of the square lattice to construct the south square grid district. All quads attached to the bottom boundary of the bottom square grid district are chosen to be horizontally aligned.

- A similarly defined picture for the above wired arc.
- The four edges of $\Lambda(G)$ linking those arcs opposite colors, containing respectively $a^\delta = (-3; \frac{1}{2}) + \tilde{o}_{\delta\to0}(1)$, $b^\delta = (-3; \frac{-1}{2}) + \tilde{o}_{\delta\to0}(1)$, $c^\delta = (3; \frac{-1}{2}) + \tilde{o}_{\delta\to0}(1)$ and finally $d^\delta = (3; \frac{1}{2}) + \tilde{o}_{\delta\to0}(1)$.

The required picture is sufficient to fill in the hypotheses used in the proof of Theorem 1.1.

5. Construction of the embedding in known setups and further perspectives

In this short section, we explain in greater details how the s-embedding setup applies in already known and new contexts.

5.1. **Description of the embedding procedure in several cases**

. Critical isoradial lattice

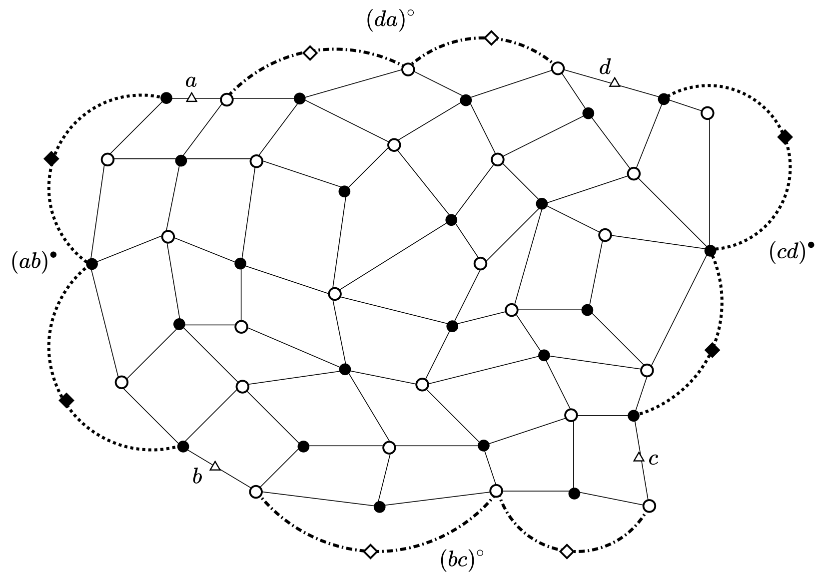

FIGURE 7. Domain $(\Omega_\delta; a^\delta, b^\delta, c^\delta, d^\delta)$ seen as a discrete simply domain in $\mathcal{S}^\delta$ with two wired boundary arcs $(b^\delta c^\delta)^\circ$, $(d^\delta a^\delta)^\circ$ (wired with irregular dashes) and a two dual wired boundary arcs $(c^\delta d^\delta)^\bullet$ and $(a^\delta b^\delta)^\bullet$ (wired with regular dashes). The wired boundary half quads are filled in white while the free boundary half quads are filled in black.

Recall that an isoradial embedding is an embedding in the plane such that each face is inscribed in a circle, the center of each circle is inside the face, and all the circles radii are equal (say to δ). In that case, the graph $\Lambda(G)$ is a *rhombus* tiling. When the grid is equipped with critical Z-invariant weights (invariant under star-triangle transformations, see [3, 4]), counterparts to Theorems 1.1 and 1.2 were proven in [14], under the bounded-angle assumption, starting from a solution to (2.6) being $X(c) := \eta_c$, defined in (2.7), with the arbitrary embedding $\mathcal{S}$ being in that case one isoradial embedding. Removing the bounded angles assumption allows to apply directly [20, Proposition 5.1] to derive the box crossing property for the Quantum Ising model on $\mathbb{Z} \times \mathbb{R}$.

Massive isoradial lattice

In this case, we still work on an isoradial grid but this time being equipped with near critical weights, with a nome $q = \frac{m\delta}{2}$ (see [41, Section 1] or [11, Equation (1.1)-(1.3)]) on a grid of mesh size δ, that satisfies the bounded angle property. In the classical formulation of the Ising model, it corresponds to looking at the homogeneous model on $\frac{1}{n}\mathbb{Z}^2$ at the uniform inverse temperature $\beta_c + \frac{m}{2n}$. In this framework, the parameter m is called the mass and measures how far from criticality is the system. Using the so called discrete exponentials introduced and studied in [3, 4] as solution to (2.6), one can re-embed the near critical model and construct an s-embedding as done in details in [11, Section 3.3]. In particular, in the embedding given in [11, Theorem 3.19], the space-like surface constructed in the Minkowski space $\mathbb{R}^{2,1}$ (see discussion in the next sub-section) is *of mean-curvature equal to the* *mass* m (scaled in the surface embedded in $\mathbb{R}^{2,1}$). It is not hard to see in the formula [11, Equation (3.12)] that, when the mass $|m| \to \infty$, the smallest possible Lipschitz constant for the origami map $\mathcal{Q}^\delta$ gets closer and closer to 1. This fact should be compared with the results of [41, Section 6] that state that crossing probabilities go respectively to $0/1$ when $|m| \to \infty$, approaching the off-critical regime. In this case, crossing estimates are not bounded away from 0 and 1 while the optimal Lipschitz constant for the origami map gets closer and closer to 1.

Critical double-periodic lattice

In that setup, the criticality condition was derived in [15] by Cimasoni and Duminil-Copin. The question of finding an embedding for the critical model was settled by Chelkak in [5, Lemma 2.3]. In this lemma, it is used that the real linear vector space of periodic solutions to (2.6) is two dimensional, and one cleverly chosen complex combination of a basis of that vector space to construct the canonical embedding, which leads to a double periodic picture in the $\mathcal{S}$ plane. Let us mention that from the crossing estimates perspective, such clever choice is *not* needed as any non trivial complex linear combination of that basis of solution leads to a proper non-degenerate s-embedding, which constructs an origami functions which grows linearly with a Lipschitz constant strictly smaller than 1.

Lis' circle patterns

In [33], Lis introduces the notion of Ising model on circle patterns depending on some inverse temperature β, the latter being constructed as follows (translating the notation of the original paper to our framework). A circle pattern is a pair of planar graphs $G = (G^\bullet, E)$ and $G^\star = (G^\circ, E^\star)$ mutually dual to each other, embedded in the complex plane in such a way that each face of $G^\star$ is inscribed in a circle inside the closure of the face, and the vertices of G lie at the center of the circles. In that case, the faces of the graph $\Lambda(G) = G^\circ \cup G^\bullet$ are *kites*, which fits into our s-embeddings framework and the weights fit at the inverse temperature $\beta = 1$. Seen as an s-embedding, the origami map is constant (set e.g. to vanish) on $\mathcal{S}(G^\circ)$ and takes the edge-length of the kites on $\mathcal{S}(G^\bullet)$. In particular in the case of graphs with non-smashed angles and comparable edge-length (assumption $\text{Unif}(\delta)$, in [5]), one can easily see that $\mathcal{Q}^\delta = O(\delta)$. Our theorem allows to study the model without those bounded angle and edge-length comparability properties, in particular in the case of *circle packings* presented in [33, Example 2], coming potentially from random graphs as one can see in the next example.

Circle patterns coming from random planar triangulation

We continue the previous discussion, but this time using Lis' circle patterns coming from a random triangulation. We keep here exactly the notations of [25]. The discrete mating-of-trees, introduced by Duplantier, Gwynne, Miller and Sheffiled [22, 26] is a model of random triangulation in the plane of the vertex set $\varepsilon\mathbb{Z}$. This random triangulation, indexed by a positive number $\varepsilon > 0$ and $\mathcal{G}^\varepsilon$, is built using a pair of correlated Brownian motions (see [25, Section 1.2] for a short introduction to that setup), and belongs to the universality class of a γ-LQG surface (with $\gamma \in]0;2[$). Doing minor modification procedures as in [25, Section 1.2] (at the boundary of a finite set and removing some double edges), one can extract from $\mathcal{G}^\varepsilon$ a finite triangulation with boundary, denoted $(\mathcal{G}_2^\varepsilon, \rho)$. The graph $(\mathcal{G}_2^\varepsilon, \rho)$ can then be circle packed in the unit disc $\mathbb{D}$, uniquely up to rotations. This circle packing is denoted by $\mathcal{P}_\rho^\varepsilon = \{C_v\}_{v \in \mathcal{V}\mathcal{G}_2^\varepsilon}$, where the circle C_ρ is centered at the origin. Theorem

1.4 of [25] ensure that, with probability $1-o_{\varepsilon\to 0}(1)$, the maximal size of one circle in $\mathcal{P}^\varepsilon_\rho$ is of order $O(\log(\varepsilon^{-1})^{-1})$, with the constant O and o only depend on $\gamma\in]0;2[$.

We are now going to use Lis' critical weights on circle patterns to decorate the faces of this circle packed triangulation (see Figure **??**) with an Ising model. Set the vertices of $G^\bullet$ to be located at the center of the circles of $\mathcal{P}^\varepsilon_\rho$ and while the vertices of G° correspond to the center of the circles of the dual triangulation, which correspond here to the centers of the inscribed circles attached to faces of that triangulation. This means that each vertex of G° in fact corresponds exactly to one face of the original circle packing. This context falls into Lis' framework of circle patterns, and the graph $\Lambda(G)$ is indeed formed of kites. We can then assign a coupling constant $x(e)=\tan\frac{\theta_e}{2}$ to the edge of the triangulation associated to the quad $z_e\in\Lambda(G)$, where the abstract angle θ_e is given by the angle formula (2.11).

Set $\delta=-\log(\varepsilon^{-1})^{-1}$. Then with probability $1-o_{\delta\to 0}(1)$, one has the origami map that satisfies $\mathcal{Q}=O(\delta)$. One still needs to check the $\textsc{Exp-Fat}(\delta)$ condition to be able to apply Theorem 1.2. This can done using the SLE/LQG estimate coming from [28, Proposition 6.2], that state that with probability $1-o_{\varepsilon\to 0}(1)$, the triangulation contains at most a polynomial power of $\log(\varepsilon)^{-1}$ vertices. In particular the ensures that, with probability going to 1 as δ goes to 0, the assumption $\textsc{Exp-Fat}(\delta)$ is fullfiled.

In conclusion, decorating the circle packing $\mathcal{P}^\varepsilon_\rho$ with weights coming naturally from the associated circle pattern, the graph satisfies, with probability $1-o_{\varepsilon\to 0}(1)$, the usual RSW property inside $\mathbb{D}(0,\frac{3}{4})$.

Layered model in the zig-zag grid. We discuss here the notion of s-embedding attached to the so called Ising model on the zig-zag lattice, defined and studied in greater details in [10, Section 5.2] . One can start with the rotated square grid (by $\frac{\pi}{4}$) and consider the Ising model on faces of that graph, chosen with all coupling constants attached to the edges separating the spins of two neighboring verticals columns C_k and C_{k-1} being the same and equal to some x_k. The collection of coupling constants $(x_k)_{k\in\mathbb{Z}}=(\tan(\theta_k))_{k\in\mathbb{Z}}$ defines an Ising model on the faces of $e^{i\frac{\pi}{4}}\mathbb{Z}^2$. One natural question is to find an s-embedding attached to this model and describe one of its realizations in the plane. It is possible to make such a construction using simple Euclidean geometrical tool as in [10, Figure 5] by pasting layers of tangential quadrilaterals all having a radius of inscribed circle equal to 1. In that case, the origami map is rather easy to compute and gives rise to an explicit formula. The vertical increments of the origami map between vertices of the same color in $\mathcal{S}(\Lambda(G))$ vanishes exactly, while the horizontal ones for $\mathcal{S}$ and $\mathcal{Q}$ between the columns $\mathcal{S}(C_l)$ and $\mathcal{S}(C_n)$ are given by the formulae (see [10, Section 5.2])

$$\mathcal{S}(C_n)-\mathcal{S}(C_l)=\sum_{k=l}^{n}\prod_{p=l+1}^{k}\tan^2(\theta_p)+\sum_{k=l}^{n}\prod_{p=l+1}^{k}\cot^2(\theta_p) \tag{5.1}$$

$$\mathcal{Q}(C_n)-\mathcal{Q}(C_l)=\sum_{k=l}^{n}\prod_{p=l+1}^{k}\tan^2(\theta_p)-\sum_{k=l}^{n}\prod_{p=l+1}^{k}\cot^2(\theta_p) \tag{5.2}$$

In particular, provided that in the regime $n\to\infty$, the ratios $\frac{\sum_{k=1}^{n}\prod_{p=1}^{k}\tan^2(\theta_p)}{\sum_{k=1}^{n}\prod_{p=1}^{k}\cot^2(\theta_p)}$ and $\frac{\sum_{k=l}^{n}\prod_{p=1}^{k}\tan^2(\theta_p)+\sum_{k=1}^{n}\prod_{p=1}^{k}\cot^2(\theta_p)}{n}$ remain bounded away from 0 and ∞, usual RSW property holds. This gives a concise proof of the RSW property for the homogeneous massive square lattice.

Construction of new critical grids using pairs of s-holomorphic functions

We present now a simple and new method to construct new proper s-embeddings out of already existing ones. We are grateful to Dmitry Chelkak and SC Park for discussions that lead to this construction (which will be detailed in a subsequent work, jointly with Park), and we present here its spirit. We present it in the case where the original embedding is the square lattice, but the technique applies in a fairly general setup given a sequence of proper s-embeddings satisfying Lip(κ,δ) (one should be careful with uniqueness statements in the case the limiting origami map ϑ is very rough). The first step it to discretize an holomorphic function f as a limit of s-holomorphic function $(F^\delta)_{\delta>0}$ in a fixed closed ball $\overline{U}$ in the plane. Set $I = \int f(z)dz$ the primitive of f that vanishes at one fixed point of the domain. Then consider H^δ the discrete harmonic extension of $\mathrm{Re}[I]$ using the boundary values of $\mathrm{Re}[I]$ on the boundary of $(\mathcal{S} + i\mathcal{Q}) \cap \overline{U}$, for the forward random walk associated to the Laplacian given in [5, Definition 2.15]. That random walk satisfies *uniform crossing estimates* (see [5, Section 2.3-2.6]), which ensures (using the regularity theory developed in [13, Section 6]) that the family of functions H^δ is precompact and its gradients F^δ are bounded s-holomorphic function at least in a ball twice smaller than $\overline{U}$. In its turn, this makes the family $(F^\delta)_{\delta>0}$ also precompact. It is the not hard to see that the functions H^δ and F^δ converge respectively to $\mathrm{Re}[I]$ and f.

We are now going to construct a proper s-embedding coming from a *discrete Weierstrass parametrization* of a space-like surface in $\mathbb{R}^{2,1}$, following the route of [11, Section 3.3]. Fix f and g two holomorphic functions on $\mathbb{D}$ such that $\mathrm{Im}[\overline{f}g] > 0$, respectively discretized by F^δ and G^δ. Then setting (as in [11, equation (3.11)]

$$(\mathrm{Re}[\mathcal{S}], \mathrm{Im}[\mathcal{S}], \mathcal{Q}) = \frac{1}{2}(\mathrm{Im} \int 2F^\delta G^\delta, \mathrm{Im} \int (F^\delta)^2 - (G^\delta)^2, \mathrm{Im} \int (F^\delta)^2 + (G^\delta)^2) \quad (5.3)$$

construct an s-embedding (the integration here is understood as (2.18)). Using the identification (2.14) with $\mathcal{X} = \varsigma(\mathcal{X}_f - i\mathcal{X}_g)$ and $\mathrm{Re}[\mathcal{S}_\mathcal{X}] = 2H[\mathcal{X}_f, \mathcal{X}_g]$, $\mathrm{Im}[\mathcal{S}_\mathcal{X}] = H_{\mathcal{X}_f} - H_{\mathcal{X}_g}$ and $\mathcal{Q}_\mathcal{X} = H_{\mathcal{X}_f} + H_{\mathcal{X}_g}$. It is easy to see from [5, Proposition 3.20] that all the faces of $\Lambda(G)$ in the associated s-embedding are oriented in the same way, they all satisfy an assumption of the kind Unif(δ) and that the associated s-embedding is proper provided δ is small enough (using the argument principle to prove properness [5, Proposition 3.20]).

The argument principle to ensure properness of the embedding, presented in a very complete manner in [12, Appendix] can be roughly summarized that one can derive properness of a piece of an s-embedding inside one oriented boundary contour in the abstract planar graph if this contour only winds once around a twice smaller region in the associated s-embedding realization. This can be used as a starting points for deterministic graphs with random coupling constants, in the case where one can find some solutions to (2.6) that average to the deterministic setup at large scale. We leave this remark as a starting point for further researches.

Finite graphs. We discuss now the existence of a proper s-embedding for a given finite graph, following [32, Section 7]. One of the important output of [32] is that if one starts with bipartite weighted planar graph with an outer face of degree

4, it is possible to find a t-embedding of its dual. The dimer model on faces of that t-embedding has edge weights which are gauge equivalent to edge-lengths of t-embedding. There, the construction is made by an algorithm, placing new points of the embedding step by step using Miquel's six-circles theorem. Start with a weighted finite planar graph (G,x) with a marked face which corresponds to its unbounded region of one of its embedding $\mathcal{E}$ into the plane and proceed as follows.

- Up to adding at most 3 faces to the unbounded face of $\mathcal{E}$, one can assume that the external boundary of that unbounded face in the graph (G,x) has $4n$ edges.
- Weld *abstractly* the obtained outer-face with the inner boundary of $[-2n;2n]^2\setminus[-n;n]^2$. Moreover, declare the edge-weights between the added faces to be the ones of the critical square lattice. This creates an $(\tilde{G},\tilde{x})$ and now an outer face with a boundary of $16n$ edges.
- Consider the graph $\Lambda(\tilde{G})=\tilde{G}^\bullet\cup\tilde{G}^\circ$ and declare the outer-face of that graph to be the quad of $\Lambda(\tilde{G})$ that corresponds an edge of the box Λ_{2n} (before the welding) near $(\frac{3}{2}n;\frac{3}{2}n)$.
- Now one has a bipartite graph with outer face of degree 4 and can then apply the construction of [32] to construct the associated t-embedding of the associated dimer model under the bozonisation identities of [17]. It is possible to apply [32, Section 7] and obtain a proper s-embedding whose edge weights correspond to the one of $(\tilde{G},\tilde{x})$, except at that new marked faces. In particular, this provides a solution to the propagation equation (2.6) except at that marked outer face.

Extracting the picture coming associated to original part of (G,x) provides a proper s-embedding.

5.2. **Optimality of the Lip assumption and embedding in the Minkowski space.** One can wonder it if is possible to prove the same RSW type estimate without an assumption of the kind $\textsc{Lip}(\kappa,\delta)$. The answer to this question is negative and proves the optimality of this kind of assumption. Consider first the off-critical homogeneous model on the square lattice (at a fixed $\beta\neq\beta_c$). The RSW box-crossing property classically fails there. Using formulae in the homogeneous layered model presented above (see also [5, Figure 2]), one easily sees that $\limsup_{z\to\infty}|\frac{\mathcal{Q}(z)}{\mathcal{S}(z)}|=1$, which indicates that the assumption $\textsc{Lip}(\kappa,\delta)$ fails, together with the box-crossing property. Even in the case of the critical square lattice, there is a more conceptual reason to this phenomenology passing to surfaces in the Minkowski space $\mathbb{R}^{2,1}$. As noted in [5, Remark 1.2], replacing $\mathcal{X}$ by $\tilde{\mathcal{X}}(t)=\cosh(t)\mathcal{X}+\sinh(t)\mathcal{X}$ for t in $\mathbb{R}$ constructs a new s-embedding on the plane. The functions $\mathcal{S}$ and $\mathcal{Q}$ are now replaced by $(\operatorname{Re}\mathcal{S},\operatorname{Im}\mathcal{S},\mathcal{Q})\mapsto(\cosh(2t)\operatorname{Re}\mathcal{S}+\sinh(2t)\mathcal{Q},\operatorname{Im}\mathcal{S},\sinh(2t)\operatorname{Re}\mathcal{S}+\cosh(2t)\mathcal{Q})$. When viewed as a space-like surface in $\mathbb{R}^{2,1}$, the surfaces $(\mathcal{S}_{\mathcal{X}},\mathcal{Q}_{\mathcal{X}})$ and $(\mathcal{S}_{\tilde{\mathcal{X}}(t)},\mathcal{Q}_{\tilde{\mathcal{X}}(t)})$ are isometric in $\mathbb{R}^{2,1}$.

Consider now the critical square lattice of mesh size $\sqrt{2}$, with its usual square embedding. In that case $\mathcal{Q}=1$ on $\mathcal{S}(G^\bullet)$ and $\mathcal{Q}=0$ on $\mathcal{S}(G^\circ)$. One can apply the transformation given above with a large t. In that case, one can make the surface $(\mathcal{S}_{\tilde{\mathcal{X}}(t)},\mathcal{Q}_{\tilde{\mathcal{X}}(t)})$ becomes closer and closer to the light cone in $\mathbb{R}^{2,1}$, meaning the optimal Lipschitz constant for the associated origami map gets closer and closer to 1 as $t\to\infty$. Considering an $[0;n]^2$ box over this newly constructed s-embedding

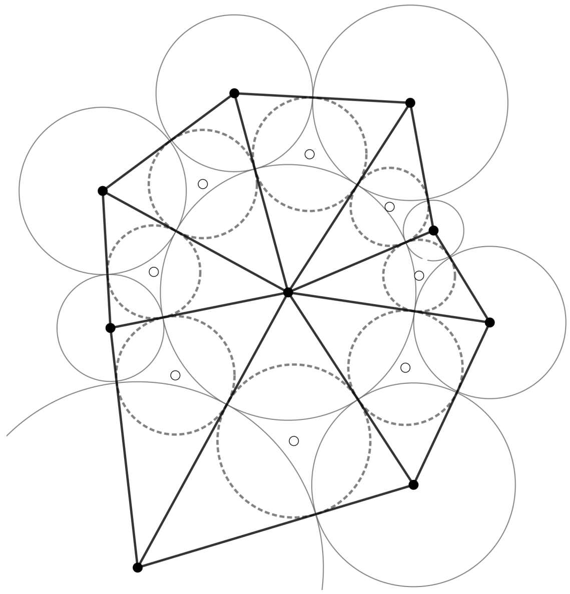

FIGURE 8. Circle pattern associated to a circle packing. The edges of the triangulation are in solid black, the circles of the packing are in solid grey, while the circles of the dual packing are in dashed grey. Each edge of the triangulation corresponds to a kite in $\Lambda(G)$, which allows to decorate faces of the triangulation with Ising weights coming from (2.11).

in the $\mathcal{S}_{\tilde{\mathcal{X}}(t)}$ plane, it corresponds to a smashed rectangle $[0;\frac{1}{\cosh(2t)}n]\times[0;n]$ in the $\mathcal{S}_{\mathcal{X}}$ plane, where the RSW property fails as $t\to\infty$. Such stretching (replacing $\mathcal{X}$ by $\mathcal{X}+|t|\overline{\mathcal{X}}$ with $|t|\to 1$) leading to an optimal Lipschitz constant close to 1 is a general fact for proper s-embeddings and is not compatible with RSW type estimates. The two previous example ensure that the assumption of the kind $\textsc{Lip}(\kappa,\delta)$ is necessary to prove our results in the general s-embeddings setup.

References

[1] Arseniy Akopyan and Alexander Bobenko. "Incircular nets and confocal conics". In: *Transactions of the American Mathematical Society* 370.4 (2018), pp. 2825–2854.

[2] Kari Astala, Tadeusz Iwaniec, and Gaven Martin. "Elliptic Partial Differential Equations and Quasiconformal Mappings in the Plane (PMS-48)". In: *Elliptic Partial Differential Equations and Quasiconformal Mappings in the Plane (PMS-48)*. Princeton University Press, 2008.

[3] Cédric Boutillier, Béatrice de Tiliere, and Kilian Raschel. "The Z-invariant massive Laplacian on isoradial graphs". In: *Inventiones mathematicae* 208.1 (2017), pp. 109–189.

[4] Cédric Boutillier, Béatrice de Tilière, and Kilian Raschel. "The Z-invariant Ising model via dimers". In: *Probability Theory and Related Fields* 174.1 (2019), pp. 235–305.

[5] Dmitry Chelkak. "Ising model and s-embeddings of planar graphs". In: *arXiv preprint arXiv:2006.14559* (2020).

[6] Dmitry Chelkak. "Planar Ising model at criticality: state-of-the-art and perspectives". In: *Proceedings of the International Congress of Mathematicians—Rio de Janeiro 2018. Vol. IV. Invited lectures.* World Sci. Publ., Hackensack, NJ, 2018, pp. 2801–2828.

[7] Dmitry Chelkak, David Cimasoni, and Adrien Kassel. "Revisiting the combinatorics of the 2D Ising model". In: *Annales de l'Institut Henri Poincaré D* 4.3 (2017), pp. 309–385.

[8] Dmitry Chelkak, Clément Hongler, and Konstantin Izyurov. "Conformal invariance of spin correlations in the planar Ising model". In: *Ann. of Math. (2)* 181.3 (2015), pp. 1087–1138. ISSN: 0003-486X. DOI: `10.4007/annals.2015.181.3.5`. URL: `http://dx.doi.org/10.4007/annals.2015.181.3.5`.

[9] Dmitry Chelkak, Clément Hongler, and Konstantin Izyurov. "Correlations of primary fields in the critical Ising model". In: *arXiv preprint arXiv:2103.10263* (2021).

[10] Dmitry Chelkak, Clément Hongler, and Rémy Mahfouf. "Magnetization in the zig-zag layered Ising model and orthogonal polynomials". In: *arXiv:1904.09168* (Apr. 2019).

[11] Dmitry Chelkak, Konstantin Izyurov, and Rémy Mahfouf. "Universality of spin correlations in the Ising model on isoradial graphs". In: *arXiv preprint arXiv:2104.12858* (2021).

[12] Dmitry Chelkak, Benoît Laslier, and Marianna Russkikh. "Bipartite dimer model: perfect t-embeddings and Lorentz-minimal surfaces". In: *arXiv preprint arXiv:2109.06272* (2021).

[13] Dmitry Chelkak, Benoît Laslier, and Marianna Russkikh. "Dimer model and holomorphic functions on t-embeddings of planar graphs". In: *arXiv preprint arXiv:2001.11871* (2020).

[14] Dmitry Chelkak and Stanislav Smirnov. "Universality in the 2D Ising model and conformal invariance of fermionic observables". In: *Invent. Math.* 189.3 (2012), pp. 515–580. ISSN: 0020-9910. DOI: `10.1007/s00222-011-0371-2`. URL: `http://dx.doi.org/10.1007/s00222-011-0371-2`.

[15] David Cimasoni and Hugo Duminil-Copin. "The critical temperature for the Ising model on planar doubly periodic graphs". In: *Electron. J. Probab.* 18 (2013), no. 44, 18. ISSN: 1083-6489. DOI: `10.1214/EJP.v18-2352`. URL: `https://doi.org/10.1214/EJP.v18-2352`.

[16] Viktor S Dotsenko and Vladimir S Dotsenko. "Critical behaviour of the phase transition in the 2D Ising model with impurities". In: *Advances in Physics* 32.2 (1983), pp. 129–172.

[17] Julien Dubédat. "Exact bosonization of the Ising model". In: *arXiv e-prints*, arXiv:1112.4399 (Dec. 2011), arXiv:1112.4399. arXiv: `1112.4399 [math.PR]`.

[18] Hugo Duminil-Copin. "Parafermionic observables and their applications to planar statistical physics models". In: *Ensaios Matematicos* 25 (2013), pp. 1–371.

[19] Hugo Duminil-Copin, Christophe Garban, and Gábor Pete. "The near-critical planar FK-Ising model". In: *Communications in Mathematical Physics* 326.1 (2014), pp. 1–35.

[20] Hugo Duminil-Copin, Jhih-Huang Li, and Ioan Manolescu. "Universality for the random-cluster model on isoradial graphs". In: *Electron. J. Probab.* 23 (2018), Paper No. 96, 70. DOI: `10.1214/18-EJP223`. URL: `https://doi.org/10.1214/18-EJP223`.

[21] Hugo Duminil-Copin, Ioan Manolescu, and Vincent Tassion. "Planar random-cluster model: fractal properties of the critical phase". In: *Probability Theory and Related Fields* 181.1 (2021), pp. 401–449.

[22] Bertrand Duplantier, Jason R Miller, and Scott Sheffield. "Liouville quantum gravity as a mating of trees". In: *Astérisque* 427 (2021).

[23] Bertrand Duplantier and Scott Sheffield. "Liouville quantum gravity and KPZ". In: *Inventiones mathematicae* 185.2 (2011), pp. 333–393.

[24] S. Friedli and Y. Velenik. *Statistical mechanics of lattice systems*. A concrete mathematical introduction. Cambridge University Press, Cambridge, 2018, pp. xix+622. ISBN: 978-1-107-18482-4.

[25] Ori Gurel-Gurevich, Daniel C Jerison, and Asaf Nachmias. "A combinatorial criterion for macroscopic circles in planar triangulations". In: *arXiv preprint arXiv:1906.01612* (2019).

[26] Ewain Gwynne, Jason Miller, and Scott Sheffield. "The Tutte embedding of the mated-CRT map converges to Liouville quantum gravity". In: (2021).

[27] Nina Holden and Xin Sun. "Convergence of uniform triangulations under the Cardy embedding". In: *Acta Mathematica* 230.1 (2023), pp. 93–203.

[28] Nina Holden and Xin Sun. "SLE as a mating of trees in Euclidean geometry". In: *Communications in Mathematical Physics* 364.1 (2018), pp. 171–201.

[29] Clément Hongler and Stanislav Smirnov. "The energy density in the planar Ising model". In: *Acta Math.* 211.2 (2013), pp. 191–225. ISSN: 0001-5962. DOI: `10.1007/s11511-013-0102-1`. URL: `http://dx.doi.org/10.1007/s11511-013-0102-1`.

[30] Leo P. Kadanoff and Horacio Ceva. "Determination of an operator algebra for the two-dimensional Ising model". In: *Phys. Rev. B (3)* 3 (1971), pp. 3918–3939. ISSN: 0163-1829.

[31] Antti Kemppainen and Stanislav Smirnov. "Conformal invariance in random cluster models. II. Full scaling limit as a branching SLE". In: *arXiv preprint arXiv:1609.08527* (2016).

[32] Richard Kenyon et al. "Dimers and Circle patterns". In: *arXiv e-prints*, arXiv:1810.05616 (2018), arXiv:1810.05616. arXiv: `1810.05616 [math-ph]`.

[33] Marcin Lis. "Circle patterns and critical Ising models". In: *Communications in Mathematical Physics* 370.2 (2019), pp. 507–530.

[34] Rémy Mahfouf. "Universalité du modèle d'Ising au-delà de cadre isoradial". PhD thesis. Université Paris-Saclay, 2022.

[35] Rémy Mahfouf and Sung Chul Park. "From the Ising model to the Lorentz Geometry I: Convergence of fermionic observables and crossing probabilities". In: (In preparation).

[36] Rémy Mahfouf and Sung Chul Park. "From the Ising model to the Lorentz Geometry II: Convergence of the energy density". In: (In preparation).

[37] Barry M. McCoy and Tai Tsun Wu. *The two-dimensional Ising model*. Second. Corrected reprint of [MR3618829], with a new preface and a new chapter (Chapter XVII). Dover Publications, Inc., Mineola, NY, 2014, pp. xvi+454. ISBN: 978-0-486-49335-0; 0-486-49335-0.

[38] Christian Mercat. "Discrete Riemann surfaces and the Ising model". In: *Comm. Math. Phys.* 218.1 (2001), pp. 177–216. ISSN: 0010-3616. DOI: `10.1007/s002200000348`. URL: `http://dx.doi.org/10.1007/s002200000348`.

[39] John Palmer. *Planar Ising Correlations*. Vol. 49. Springer Science & Business Media, 2007.

[40] S. C. Park. "Massive Scaling Limit of the Ising Model: Subcritical Analysis and Isomonodromy". In: *arXiv e-prints*, arXiv:1811.06636 (Nov. 2018), arXiv:1811.06636. arXiv: `1811.06636 [math.PR]`.

[41] SC Park. "Convergence of fermionic observables in the massive planar FK-Ising model". In: *arXiv preprint arXiv:2103.04649* (2021).

[42] Jacques HH Perk. "Quadratic identities for Ising model correlations". In: *Physics Letters A* 79.1 (1980), pp. 3–5.

[43] Stanislav Smirnov. "Conformal invariance in random cluster models. I. Holomorphic fermions in the Ising model". In: *Ann. of Math. (2)* 172.2 (2010), pp. 1435–1467. ISSN: 0003-486X. DOI: `10.4007/annals.2010.172.1441`. URL: `https://doi.org/10.4007/annals.2010.172.1441`.

[44] Stanislav Smirnov. "Towards conformal invariance of 2D lattice models". In: *In* International Congress of Mathematicians. Vol. II*, pages 1421–1451. Eur. Math. Soc., Zürich* (2006).

[45] JS Wang et al. "The Two-Dimensional Random Bond Ising Model at Criticality—A Monte Carlo Study". In: *Europhysics Letters* 11.4 (1990), p. 301.